Received: 8 December 2023 | Revised: 18 January 2024 | Accepted: 24 January 2024

DOI: 10.1002/agt2.520

Aggregate WILEY

RESEARCH ARTICLE

Gd-based molecular coolants: Aggregating for better magnetocaloric effect

Yuan-Qi Zhai[1,2] | **Wei-Peng Chen**[1,2] | **Marco Evangelisti**[3] | **Zhendong Fu**[4] | **Yan-Zhen Zheng**[1,2]

[1]Department of Hepatobiliary Surgery, Institute of Advanced Surgical Technology and Engineering, The First Affiliated Hospital of Xi'an Jiaotong University, Xi'an, Shaanxi, P. R. China

[2]Frontier Institute of Science and Technology, Xi'an Key Laboratory of Electronic Devices and Materials Chemistry, School of Chemistry, Xi'an Jiaotong University, Xi'an, Shaanxi, P. R. China

[3]Instituto de Nanociencia y Materiales de Aragón, CSIC & Universidad de Zaragoza, Zaragoza, Spain

[4]Songshan Lake Materials Laboratory, Dongguan, P. R. China

Correspondence
Wei-Peng Chen and Yan-Zhen Zheng, Department of Hepatobiliary Surgery and Institute of Advanced Surgical Technology and Engineering, The First Affiliated Hospital of Xi'an Jiaotong University, Xi'an, Shaanxi 710061, P. R. China.
Email: sxchenweipeng@163.com and zheng.yanzhen@xjtu.edu.cn

Funding information
National Natural Science Foundation of China, Grant/Award Numbers: 21971203, 22375157; State Key Laboratory of Electrical Insulation and Power Equipment, Grant/Award Numbers: EIPE23402, EIPE23405; Special Support Plan of Shaanxi Province for Young Top-notch Talent and the Fundamental Research Funds for Central Universities, Grant/Award Number: xtr052023002; Medical-Engineering Cross Project of the First Affiliated Hospital of XJTU, Grant/Award Number: QYJC02; Spanish MICINN, Grant/Award Number: PID2021-124734OB-C21; "Scientists + Engineers" Team Building Project of Qin Chuang Yuan, Grant/Award Number: 2022KXJ-088

Abstract

Two series of 3d-Gd mixed-metal phosphonate complexes with either only two gadolinium centers such as $\{Gd_2\}$, $\{Ni_2Gd_2\}$, $\{Co_4Gd_2\}$, $\{Co_8Gd_2\}$, $\{Fe_6Gd_2\}$, and $\{Fe_{17}Gd_2\}$ or more than two gadoliniums such as $\{Co_8Gd_4\}$, $\{Mn_8Gd_4\}$, $\{Co_4Gd_6\}$, $\{Mn_4Gd_6\}$, $\{Co_6Gd_8\}$, $\{Ni_5Gd_8\}$, $\{Ni_6Gd_6\}$, $\{Co_8Gd_8\}$, and $\{Mn_9Gd_9\}$ have been solvothermally prepared and magnetothermally studied. The nearly identical environments of the Gd(III) dimer in the first series allow us to qualitatively analyze the effect of magnetic exchange coupling on the magnetocaloric effect (MCE). By doubling, tripling, or quadrupling of the Gd(III) centers, the second series of 3d-Gd mixed-metal complexes was built to further test the other effects of exchange couplings on MCE in more complicated circumstances. For the antiferromagnetic coupling cases, the results are nearly identical but diversify when topological spin frustrations are created, whose massive low-lying excited spin states help enhance MCE. For presumably ferromagnetically coupled ones, albeit are rare in phosphonate complexes, they do exhibit excellent MCE. Meanwhile, the complexes with weakly coupled metal centers serve as excellent examples for studying the effect of molecular mass on MCE when its magnitude is expressed in the unit of Joule per kilogram, from which we can see the values are directly proportional to the percentage of the Gd(III) ions in molecular weight.

KEYWORDS
3d-4f, lanthanide, magnetocaloric effect, phosphonate, refrigerant

1 | INTRODUCTION

Magnetic cooling is a technique that exploits the magnetocaloric effect (MCE), which was first discovered in metallic nickel by Weiss and Piccard in 1917, to take away the heat.[1] This is an attractive green technology for acquiring low temperature because of no emission of any hazardous gas such as freon into the atmosphere compared to the traditional vapor compression technique.[2] The figure-of-merits of MCE are the change of magnetic entropy (ΔS_m) and adiabatic temperature (ΔT_{ad}) under applied magnetic field (ΔB). For the application of magnetic cooling, two temperature regions are of particular interest, namely, the near room temperature region for daily-life cooling and the low-temperature region (<20 K) to replace helium as a coolant.[3] Although tremendous effort has been paid during the past 130 years, this appreciated technology has yet to be extensively applied. Two major reasons may be accountable: (1) the efficiency of

the cooling has not met the standard of refrigeration; and (2) the cost of the current magnetic refrigerants is still too high, among which the priority is to solve the first problem.

In the past, excellent magnetic refrigerants were almost made of gadolinium(III) compounds by taking the advantage of large spin state ($s = 7/2$) of this ion. But the recipes were usually obtained by trial-and-error, including the famous giant MCE materials, for example, $Gd_5Si_2Ge_2$[4] for room temperature cooling, $Gd_3Ga_5O_{12}$ (GGG)[5] and its iron-substituted derivatives $Gd_3(Ga_{1-x}Fe_x)_5O_{12}$ (GGIG)[6] for low-temperature cooling, etc. Because all of these materials are bulky with periodic but infinite structures, the magnetic exchange couplings are strongly correlated and impossible to be quantitatively resolved. This is believed to be one of the major reasons that prevent the in-depth understanding of the giant MCE mechanism among these materials; thus, the rational guidance of material preparation is still in its infancy.

Magnetic exchange couplings are considered to be the strength to aggregate two or more magnetic centers in a cluster and are an effective way to enhance MCE. To accurately acquire the information of the magnetic exchange couplings and their influence on MCE, the system has to be quantum mechanically solvable; thus, finite size and homogeneous distribution are essential. The recent emergences of the molecular magnetic coolants[7–9] that contain stoichiometric inorganic–organic components with uniformed size and countable magnetic centers are promising to solve these problems. Especially, the polymetallic coordination clusters, as a kind of special aggregates with appealing molecular structures and uniform size, which are constructed via self-assembly under the assistance of N, O-ligands, small anionic bridging groups (OH^-, O^{2-}, CH_3COO^-), and anionic templates, have also been paid much attention due to their potential applications in energy-efficient and environmentally friendly cryogenic refrigerators. However, due to the formation of massive matrix for impractical diagonalization, subtle magnetic studies of many molecular coolants are virtually infeasible. Only a few examples are available, including the first investigated cluster $\{Mn_{12}\}$,[10] our previously reported aggregates $\{Fe_{14}\}$[11] and $\{Ni_6Ln_6\}$,[12] and the recently reported polymetallic complex $\{Gd_4M_8\}$.[13] These thorough studies are indeed very useful in revealing the influence of magnetic coupling on MCE in many ways, but the rational design of such proper systems remains challenging.

As we can see that the first two molecules, $\{Mn_{12}\}$ and $\{Fe_{14}\}$, actually take the advantage of a well-defined ground spin state so that the Hamiltonian can be largely simplified when the only populated state is considered to contribute to MCE. While the last two systems, $\{Ni_6Ln_6\}$ and $\{Gd_4M_8\}$, are very similar, both benefited from the two swappable 4f or 3d components, one of them could be replaced by a diamagnetic counterpart, for example, Y(III) in $\{Ni_6Ln_6\}$ and Zn(II) in $\{Gd_4M_8\}$.[12,13] Obviously, without these special designs, thorough magnetic study of a molecular cooling system remains challenging.

Herein, we demonstrate another way to qualitatively analyze the magnetic exchange coupling effects on MCE. By judicious choice of a series of 3d–4f mixed-metal complexes[14,15] with only two gadolinium centers, such as $\{Gd_2\}$, $\{Co_4Gd_2\}$, $\{Co_8Gd_2\}$, $\{Fe_6Gd_2\}$, and $\{Fe_{17}Gd_2\}$, we are able to analyze the magnetic interactions on MCE. Furthermore, by doubling, tripling, or quadrupling the Gd(III) centers, another series of complexes, namely, $\{Co_8Gd_4\}$, $\{Mn_8Gd_4\}$, $\{Co_4Gd_6\}$, $\{Mn_4Gd_6\}$, $\{Co_6Gd_8\}$, $\{Ni_5Gd_8\}$, $\{Ni_6Gd_6\}$, and $\{Co_8Gd_8\}$, were built to test other effects of exchange couplings on MCE in more complicated environments. In both circumstances, we found that antiferromagnetic interactions are usually negative for enhancing MCE unless otherwise topological spin frustrations are created.[16,17] Unlike the complicated effects of antiferromagnetic interactions on MCE ferromagnetic exchange coupling interactions, especially when they are weak, they are always preferred for a better MCE. Moreover, in these two series of 3d-Gd mixed-metal compounds, the complexes with weakly coupled metal centers should serve as excellent model complexes for studying the effect of molecular mass on MCE when its magnitude is expressed in the unit of J kg^{-1} K^{-1}, from which we can see that the obtained values are directly proportional to the percentage of Gd(III) ions in these complexes.

2 | SYNTHESIS

The story started from the gadolinium pivalate dimer, $[Gd_2(O_2C^tBu)_6(HO_2C^tBu)_6]$ (**1·Gd$_2$**), which we used as a starting material for synthesizing 3d-Gd mixed-metal complexes. To further bind 3d metal centers, we used phosphonate ligands with multiple coordination modes, as illustrated by the Harris notation[18] (Scheme 1).

By mixing either $Gd(NO_3)_3$ or **1·Gd$_2$** with 3d starting materials, such as $[M^{II}_2(\mu\text{-}OH_2)(O_2C^tBu)_4]\cdot(HO_2C^tBu)_4$ (M = Ni **Nipiv**; Co **Copiv**), $[Fe^{III}_3(\mu_3\text{-}O)(O_2C^tBu)_6(H_2O)_3]^{-}\cdot(O_2C^tBu)$ (**Fepiv**), and $[Mn^{II}(O_2C^tBu)_4(EtOH)]_n$ (**Mnpiv**) obtained from published methods,[19] a large amount of 3d-Gd mixed-metal complexes can be obtained by varying the synthetic conditions (Table 1 and Scheme S1).

When **Nipiv** reacts with lanthanide nitrate with base and with *tert*-butylphosphonic acid, we obtain crystals either directly from cooling the autoclaves at the end of the reaction, or by allowing the solution formed in the autoclave to stand for several days. The reactions involving gadolinium can give crystals both directly from cooling and from the filtrate. For filtrate, the tetrameric $[Et_3NH]_2[Ni_2Gd_2(\mu_3\text{-}OH)_2(piv)_{10}]$ (**2·Ni$_2$Gd$_2$**) was isolated with very low yield, while for directly cooling, large amounts of crystals of $[Ni_5Gd_8(\mu_3\text{-}OH)_7(\mu\text{-}OH_2)(O_3P\text{-}^tBu)_6(O_2C\text{-}^tBu)_{15}(MeCN)]$ (**12·Ni$_5$Gd$_8$**) were obtained. In general, Ln heavier than Sm but lighter than Tb results in direct cooling and gives crystals of $[Ni_5Ln_8(\mu_3\text{-}OH)_7(\mu\text{-}OH_2)(O_3P\text{-}^tBu)_6(O_2C\text{-}^tBu)_{15}(MeCN)]$ (**12·Ni$_5$Ln$_8$**, Ln = Sm, Eu, Gd, and Tb), while Ln heavier than Dy gives crystals of $[Ni_6Ln_8(\mu_3\text{-}OH)_8(\mu\text{-}OH_2)(O_3P\text{-}^tBu)_6(O_2C\text{-}^tBu)_{16}]$ (**12·Ni$_6$Ln$_8$**, Ln = Dy, Ho, and Y) instead. The replacement of both gadolinium source and phosphonic acid gave another series of products $[Ni^{II}_6Ln^{III}_6(OH)_2(O_3PCH_2Ph)_6(O_2C^tBu)_{16}(MeCO_2H)_2](MeCN)_4$ (**13·Ni$_6$Ln$_6$**, Ln = Gd, Dy, and Y), which has been reported previously.[12]

For the iron family, the similar reaction between **Fepiv**, lanthanide nitrate, and *tert*-butylphosphonic acid in basic condition cannot give any direct cooling product. But after filtration, the clear solution can give dark block crystals of

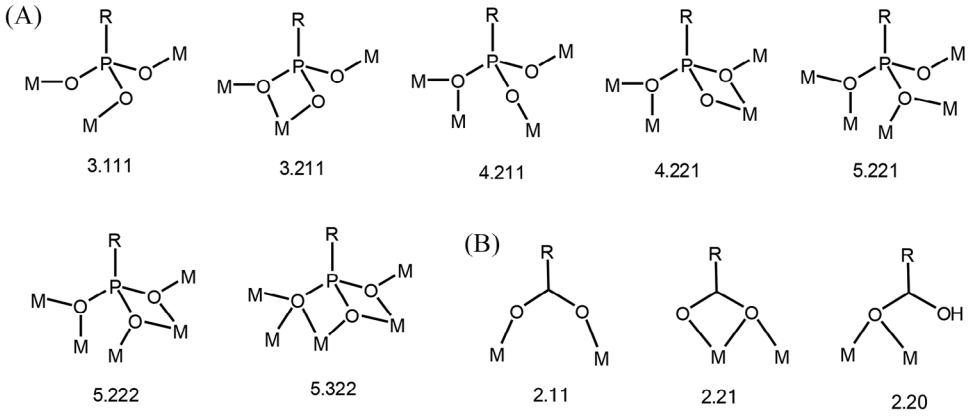

SCHEME 1 Coordination modes of phosphonate (A) and pivalate or acetate (B) in this paper, labeled with Harris notation.

TABLE 1 Synthetic summary of 3d-Gd families (**2–15**).

Complex	Phosphonate	3d stating material	Gd starting material	Base	Solvent	Produced way
2·Ni_2Gd_2	–	**Nipiv**	$Gd(NO_3)_3$	Et_3N	MeCN	Filtrate
3·Fe_6Gd_2	$PO_3{}^tBu$	**Fepiv**	$Gd(NO_3)_3$	–	MeCN	Filtrate
4·$Fe_{17}Gd_2$	$PO_3{}^tBu$	**Fepiv**	$Gd(NO_3)_3$	–	MeCN, acetone	Filtrate
5·Co_4Gd_2	$PO_3{}^tBu$	**Copiv**	$Gd(NO_3)_3$	–	MeCN	Filtrate
6·Co_8Gd_2	PO_3CH_2Ph	**Copiv**	**1·Gd_2**	–	MeCN	Filtrate
7·Co_8Gd_4	$PO_3{}^tBu$	**Copiv**	**1·Gd_2**	–	MeCN	Direct cooling
8·Mn_8Gd_4	$PO_3{}^tBu$	**Copiv**	**1·Gd_2**	–	MeCN	Direct cooling
9·Co_4Gd_6	PO_3CH_2Ph	**Copiv**	**1·Gd_2**	–	MeCN	Direct cooling
10·Mn_4Gd_6	PO_3CH_2Ph	**Mnpiv**	**1·Gd_2**	–	MeCN	Direct cooling
11·Co_6Gd_8	$PO_3{}^tBu$	**Copiv**	$Gd(NO_3)_3$	Et_3N/NaOMe	MeCN/DMF	Direct cooling
12·Ni_5Gd_8	$PO_3{}^tBu$	**Nipiv**	$Gd(NO_3)_3$	Et_3N	MeCN	Direct cooling
13·Ni_6Gd_6	PO_3CH_2Ph	**Nipiv**	$Gd(NO_3)_3$	Et_3N	MeCN	Direct cooling
14·Co_8Gd_8	$PO_3{}^tBu$	**Copiv**	$Gd(NO_3)_3$	–	MeCN	Direct cooling
15·Mn_9Gd_9	PO_3Me	**Mnpiv**	**1·Gd_2**	–	MeCN, EtOH	Direct cooling

$[Fe_6Gd_2(O_3P{}^tBu)_4(O_2C{}^tBu)_{12}(H_2O)_4(MeCN)_2]$ (**3·Fe_6Gd_2**) by several-day stay or orange prism crystals of $[Fe_{17}Ln_2(\mu_4\text{-}O)_{10}(\mu_3\text{-}O)_3(O_3P{}^tBu)_{14}(O_2C{}^tBu)_3(MeCO_2)_3]$ (**4·$Fe_{17}Ln_2$**, Ln = Sm and Gd) by layering 2 mL acetone.

The reaction of **Copiv** with different lanthanide starting materials and phosphonic acids, with or without base, can give a large number of products, which have been summarized in a previously reported paper.[8o] Herein, we highlight that the bi-gadolinium products $[Co^{II}{}_4Gd^{III}{}_2(O_3P{}^tBu)_2(O_2C{}^tBu)_{10}(MeCN)_2](MeCN)_2$ (**5·Co_4Gd_2**) and $[Co^{II}{}_8Gd^{III}{}_2(\mu_3\text{-}OH)_2(O_3PCH_2Ph)_4(O_2C{}^tBu)_{12}(HO_2CMe)_2](MeCN)_6$ (**6·Co_8Gd_2**) are, respectively, obtained by allowing the filtrate to stand several days before the isolation of higher gadolinium-number products $[Co^{II}{}_4Gd^{III}{}_6(O_3PCH_2Ph)_6(O_2C{}^tBu)_{14}(MeCN)_2]$ (**9·Co_4Gd_6**) and $[Co^{II}{}_8Gd^{III}{}_8(\mu_3\text{-}OH)_4(NO_3)_4(O_3P{}^tBu)_8(O_2C{}^tBu)_{16}]$ (**14·Co_8Gd_8**). Four-gadolinium product $[Co^{II}{}_8Gd^{III}{}_4(O_3P{}^tBu)_6(O_2C{}^tBu)_{16}]$ (**7·Co_8Gd_4**) can be obtained by reacting **Copiv** and **1·Gd_2** instead, and the highest gadolinium-percentage product $[Co^{II}{}_6Gd^{III}{}_8(\mu_3\text{-}OH)_8(O_3P{}^tBu)_6(O_2C{}^tBu)_{16}(H_2O)_2](MeCN)_2$ (**11·Co_6Gd_8**) can be obtained in extremely basic condition that accelerates the hydrolysis of lanthanide.[20]

Using the manganese starting material, **Mnpiv** can also produce a number of products, such as the teta-gadolinium $[Mn^{II}{}_8Gd^{III}{}_4(O_3P\text{-}{}^tBu)_6(O_2C\text{-}{}^tBu)_{16}]$ (**8·Mn_8Gd_4**), and the reported higher gadolinium-number products $[Mn^{II}{}_4Gd^{III}{}_6(O_3PCH_2Ph)_6(HO_2C{}^tBu)_{13}(O_2CMe)(HO_2C{}^tBu)(OH_2)_2(MeCN)_2](MeCN)_3$ (**10·Mn_4Gd_6**) and $[Mn^{II}{}_9Gd^{III}{}_9(O_3PMe)_{12}(O_2C{}^tBu)_{18}(\mu_3\text{-}OH)_{1.5}(O_2C{}^tBu)_{1.5}]$ (**15·Mn_9 Gd_9**), which can be isolated by variation of synthetic conditions, as summarized in Table 1.

2.1 | Structural description

We can divide the 3d-Gd complexes into two groups: the bi-gadolinium families (**1–6**) and the more than two gadolinium cages (**7–15**). The latter can further deviate a sub-group with core symmetry higher than C_3 (**13–15**).

2.1.1 | Structures of the bi-gadolinium families (**1–6**)

These are rare series of mixed-metal cages with only two Gd(III) centers. As shown in Figure 1A, the core of **1·Gd_2** (Table S1) features a tetra-carboxylate bridged $\{Gd_2\}$ dimer, which is covered by another four peripheral pivalates on each side. There are a total of six protonated carboxylic

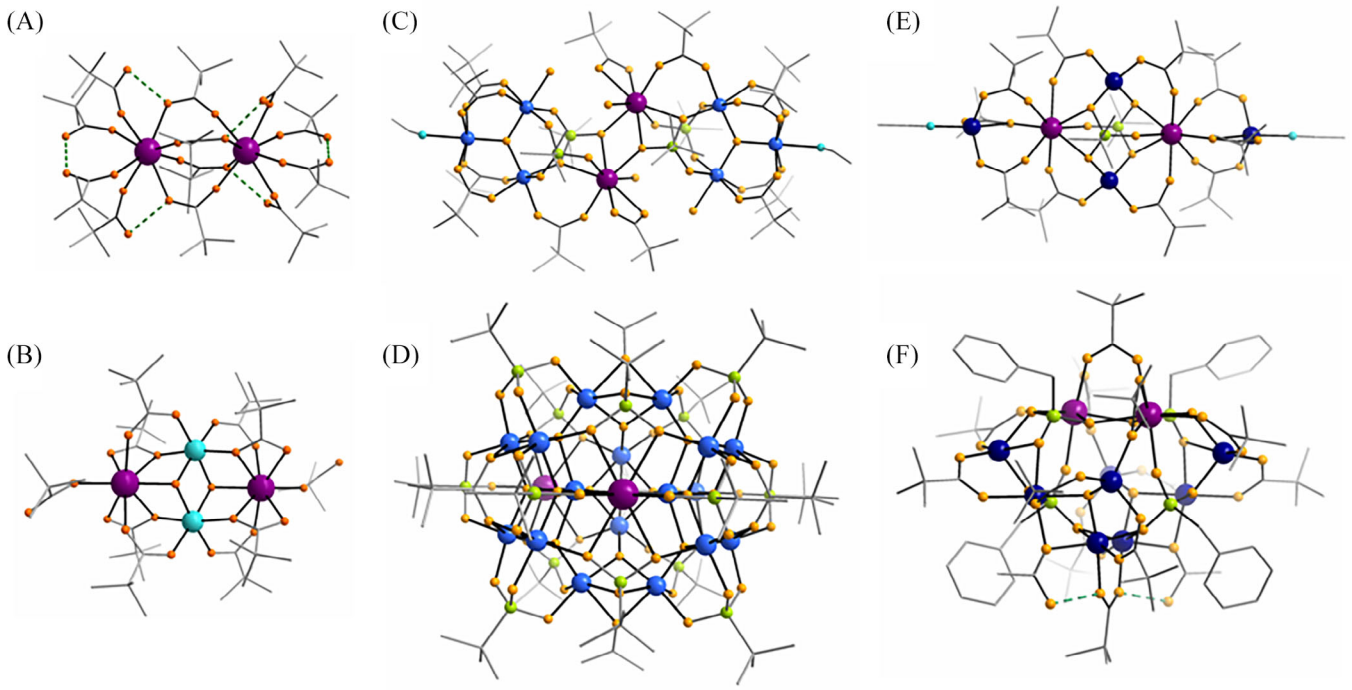

FIGURE 1 The structures of **1·Gd$_2$** (A), **2·Ni$_2$Gd$_2$** (B), **3·Fe$_6$Gd$_2$** (C), **4·Fe$_{17}$Gd$_2$** (D), **5·Co$_4$Gd$_2$** (E), and **6·Co$_8$Gd$_2$** (F). Color codes (applied to the following figures) for the structures: Ln, purple; Co, dark blue; Fe, aqua; Ni, turquoise; Mn, pink; P, green; O, orange; N, cyan; C, gray. Green dotted lines: hydrogen bonds.

ligands, albeit coordinated with the two Gd(III) centers using the mono-dentate mode, forming strong hydrogen bonds among themselves (O···O 2.42 Å), and relatively weaker hydrogen bonds with oxygen atoms from other six deprotonated pivalates (O···O 2.60 Å). Each crystallographically independent Gd(III) ion is eight-coordinated with a Gd···Gd separation of 4.51 Å.

2·Ni$_2$Gd$_2$ (Table S1) is actually a by-product when producing **12·Ni$_5$Gd$_8$**. There are no phosphonates found in the structure. As shown in Figure 1B, the two octahedral Ni(II) centers sit on the center, bridged by two μ_3-OH groups with a Ni···Ni separation of 3.20 Å. There are two Gd(III) ions sitting on each side of the Ni(II) centers. These four metal centers are coplanar, centrosymmetrically bridged by four 2.21 and four 2.11 bridging pivalates, and with the two μ_3-OH groups on each side of the plane. Note that the Ni···Gd separations are relatively short, ca. 3.44 Å, compared to the previously reported Ni–Ln mixed-metal complexes.[12] The Gd(III) ions are eight-coordinated, whose square-antiprism geometry are further completed with two terminal 1.10 pivalates. As long as these two terminal pivalates are deprotonated, the $\{Ni_2Gd_2\}$ core structure is anionic, which is counterbalanced by two lattice $[Et_3NH]^+$ cations.

3·Fe$_6$Gd$_2$ (Table S1) features a nearly unchanged motif structures compared to those of the starting materials. As shown in Figure 1C, the two triangular $[Fe_3(\mu_3\text{-}O)(O_2C^tBu)_4(H_2O)(MeCN)]$ motifs are connected to the central Gd(III) dimer mainly via the phosphonate bridges. The iron triangle remains coplanar, while two of the six pivalates are substituted by two crystallographically independent phosphonates that adopt either 3.111 or 4.221 bridging mode. The Fe(III) ions remain six-coordinated octahedral geometry, but the phosphonate-bridged triangular edge is slightly longer than those pivalate-bridged triangular edge. Although the Gd(III) ions remain eight-coordinated, the μ-O$_P$ from the 4.221 phosphonate brings the two Gd(III) ions closer than does **1·Gd$_2$** (average separations for **3·Fe$_6$Gd$_2$**, Fe···Fe 3.35 Å, Fe···Gd 4.69 Å, and Gd···Gd 3.98 Å).

4·Fe$_{17}$Gd$_2$ (Table S2) has the most metal centers among these two series of 3d-4f mixed-metal complexes. As shown in Figures 1D and 2, there are 17 Fe(III) ions that are bridged by either μ_4- or μ_3-oxo dianions. The three μ_3-oxo bridges are in the center of the $\{Fe_{17}Gd_2\}$ core (Figure 2B). One of them lies right in the middle of the cluster, bridging two Fe(III) ions and one Gd(III) ion. The other two bridge three Fe(III) ions. All the μ_3-oxo-bridged metal centers are coplanar, forming two $\{Fe_3O\}$ and one $\{Fe_2GdO\}$ triangle, and the vertexes of these three triangles are further connected with a μ_4-oxo. A total of 10 μ_4-oxo atoms are further linked with nine Fe(III) ions and one Gd(III) ion, accomplishing the central $\{Fe_{17}Gd_2(\mu_4\text{-}O)_{10}(\mu_3\text{-}O)_3\}$ core. This giant inorganic core is further capped by 14 *tert*-butylphosphonates, two 4.22 pivalates, one 3.21 pivalate, and three 2.20 acetates that are in situ formed during synthesis, which has been previously observed due to the hydrolysis of acetonitrile in solvothermal condition.[8o,8p,21] Indeed, the $\{Fe_{17}Ln_2\}$ core has low symmetry. There is no specific relationship between two lanthanide centers and the lanthanides in different coordination geometries, eight-coordinated square-antiprism for one and nine-coordinated capped square-antiprism for the other. It seems that the lanthanides are just fit to the iron-oxo cavities; thus, this core is serendipitously self-assembled after the solvothermal treatment.[22] Typical next-nearest ion separations for **4·Fe$_{17}$Gd$_2$** are 3.1–3.6 Å for Fe···Fe and for 3.4–3.6 Å for Fe···Gd.

The versatile coordination geometries of Co(II) ions led to the formation of **5·Co$_4$Gd$_2$** and **6·Co$_8$Gd$_2$**. As shown in Figure 1E,F, the central Co(II) dimeric ions of **5·Co$_4$Gd$_2$** have a four-coordinated tetrahedral geometry and the two peripheral Co(II) ions are five-coordinated. Each Gd(III) ion

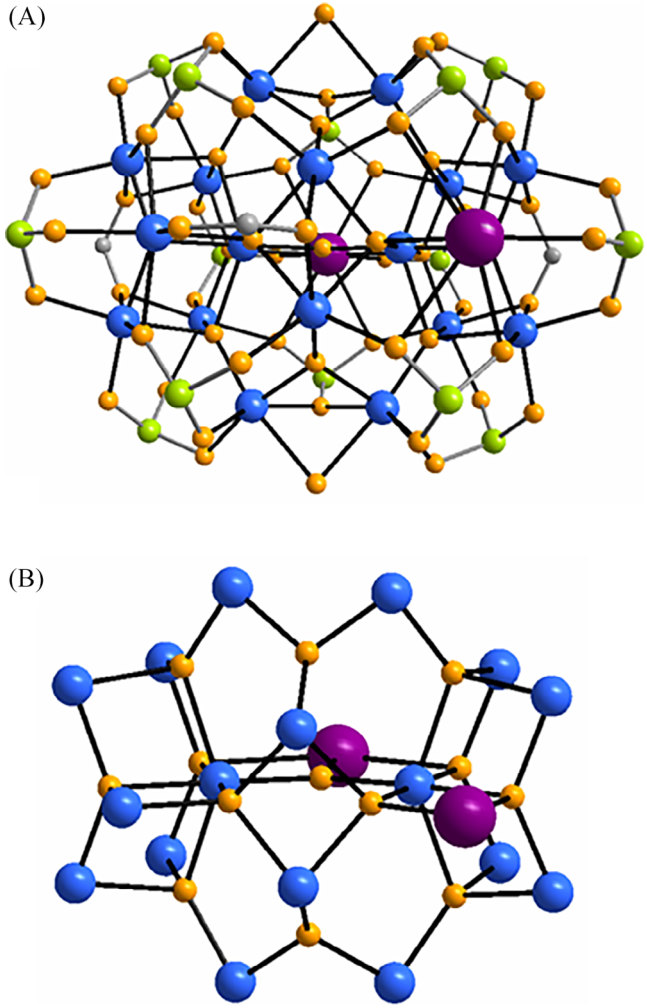

FIGURE 2 The $\{Fe_{17}Ln_2\}$ core of **4·Fe$_{17}$Ln$_2$** with (A) and without (B) phosphonates.

is surrounded by three Co(II) ions, amidst bridging ligands are two 4.221 phosphonates, four 2.11 pivalates and one 2.21 pivalate. The central Co···Gd contacts of 3.74 Å are slightly shorter than the peripheral ones at 3.92 Å. The coordination geometries of the Co(II) ions in **6·Co$_8$Gd$_2$** are more versatile. There are two μ_3-OH-bridged Co(II) triangles in the core of **6·Co$_8$Gd$_2$**. Each of them comprises two six-coordinate octahedral and one four-coordinate tetrahedral Co(II) ion. The two $\{Co_3(\mu_3\text{-OH})\}$ triangles are joined by two 5.221 phophonates and one 2.11 pivalate. These two phosphonates, together with other two 4.221 phosphonates, bind to the other two tetrahedral Co(II) ions as well as two eight-coordinate Gd(III) ions. There are also two in situ formed 2.20 acetates in the $\{Co_8Gd_2\}$ core. The average nearest Co···Ln, Ln···Ln, and Co···Co separations in **6·Co$_8$Gd$_2$** are ca. 3.72, 3.99, and 3.23 Å, respectively.

2.1.2 | Structure of the more than two gadolinium cages (**7–15**)

The second series of complexes contains more than two gadolinium ions. According to the core symmetry, we discuss the structures of these materials in the sequence of gadolinium numbers.

2.1.3 | Cores with symmetry lower than C_3 (**7–12**)

The first family has four Gd(III) ions with a general formula $[M_8Gd^{III}{}_4(O_3P\text{-}^tBu)_6(O_2C\text{-}^tBu)_{16}]$ (**M$_8$Gd$_4$**, M = Co, **7·Co$_8$Gd$_4$**; Mn, **8·Mn$_8$Gd$_4$**) (Table S2). Although the two complexes are isomorphous their structures are varied. As shown in Figure 3, the $\{Gd_2\}$ dimer of the starting material **1·Gd$_2$** is almost retained in the newly formed structure of **M$_8$Gd$_4$** except that a 4.222 phosphonate is inserted between two Gd(III) ions. This phosphonate is further bound to two M(II) ions, forming the same $\{Gd_2M_2Gd_2\}$ backbone structure in **M$_8$Gd$_4$**. But the outer M(II) metals are arranged in different ways mainly due to the disparate coordination habit of the metal ions. As shown in Figure 3B, the Co(II) ions are all four-coordinated, whereas the Mn(II) ions tend to have higher coordination numbers. Note that all the four peripheral phosphonates in **8·Mn$_8$Gd$_4$** adopt an unprecedented 5.322 binding mode. This high binding number means that the metal centers in **8·Mn$_8$Gd$_4$** are more closely related than those in the 4.221 binding mode in **7·Co$_8$Gd$_4$**. This is why the M···M contacts in **8·Mn$_8$Gd$_4$** are much shorter (average nearest M···Ln, Ln···Ln, and M···M separations are: for **7·Co$_8$Gd$_4$**, 3.83, 4.21, and 3.95 Å; for **8·Mn$_8$Gd$_4$**, 3.69, 4.23, and 3.52 Å, respectively). Except for these differences, all the metal centers in both structures are similarly coplanar.

Unlike the first family, although with the same metal numbers $\{M_4Gd_6\}$, the structures of the second family **9·Co$_4$Gd$_6$** and **10·Mn$_4$Gd$_6$** are not isomorphous. As shown in Figure 4B, the atoms in **9·Co$_4$Gd$_6$** are centrosymmetric related, but there are obviously no imposed symmetries in the core of **10·Mn$_4$Gd$_6$**, which accompanies a change in the space group from $P2_1/n$ to P-1. The reduction in symmetry can be simply viewed as the central $\{Co_2\}$ dimer in **9·Co$_4$Gd$_6$** moving to the edge of the square in **10·Mn$_4$Gd$_6$**. A full explanation for this change in structure is not obvious; however, it could be due to the size of the 3d metals. The two corner 3d metal ions are also in different coordination environment, namely, four-coordinated for **9·Co$_4$Gd$_6$** and five-coordinated for **10·Mn$_4$Gd$_6$**. The coordination modes of the phosphonates also vary between the two structures. In **9·Co$_4$Gd$_6$**, they adopt either the 4.221 or 5.222 mode, whereas in **10·Mn$_4$Gd$_6$**, they adopt the 3.211 mode as well as the 4.221 and 5.322 modes, for example, the six Gd(III) ions in **10·Mn$_4$Gd$_6$** are linked to each other through three 4.221 and two 3.211 phosphonates. Except the longer M···M separation the distances between the nearest lanthanides and the nearest M–Gd are slightly shorter in **10·Mn$_4$Gd$_6$** compared to **9·Co$_4$Gd$_6$** (average separations for **10·Mn$_4$Gd$_6$**, Gd···Gd 3.95 Å, Mn···Gd 3.87 Å, and Mn···Mn 3.95 Å; for **9·Co$_4$Gd$_6$**, Gd···Gd 4.07 Å, Co···Gd 3.89 Å, and Co···Co 3.19 Å).

When accessing Et_3N was involved in the synthesis, two new families **11·Co$_6$Gd$_8$** and **12·Ni$_5$Gd$_8$** (Table S3) can survive. As shown in Figure 5, the basic condition accelerated the hydrolysis of the metal centers, resulting in a large number of hydroxide (eight μ_3-OH groups) in both complexes. The structures of two complexes, albeit shares many common features, such as having the same number of the Gd(III) ions, hydroxyl groups, and phosphonate ligands, are indeed varied, especially the number of the 3d metal centers and their positions. At the center of **11·Co$_6$Gd$_8$** there is a C_2 symmetric $[Co^{II}{}_2Gd^{III}{}_2(\mu_3\text{-OH})_4]^{6+}$ cubane,

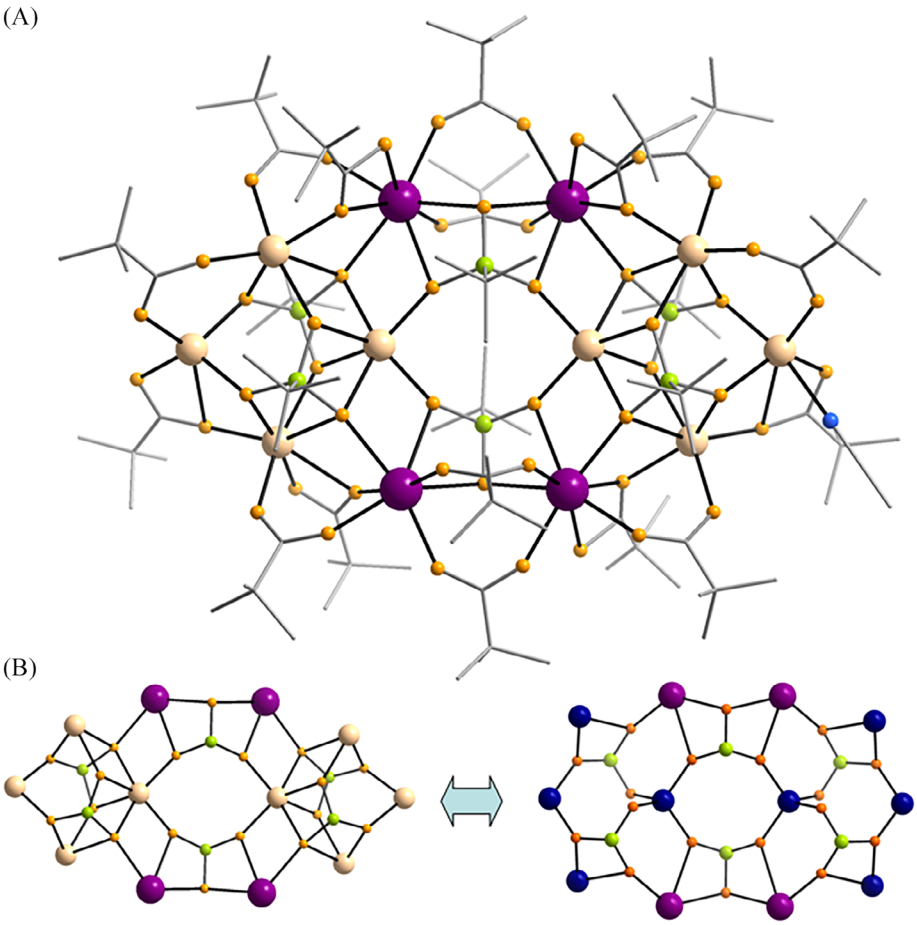

FIGURE 3 The molecular structure of **8·Mn$_8$Gd$_4$** (A) and a comparison of the cores of **8·Mn$_8$Gd$_4$** and **7·Co$_8$Gd$_4$** (B).

where is varied to an asymmetric one $[Ni^{II}{}_3Gd^{III}(\mu_3\text{-}OH)_4]^{5+}$ in **12·Ni$_5$Gd$_8$**. Surrounding these cubanes, for **11·Co$_6$Gd$_8$**, there is a $\{Co_2Ln_6O_8\}$ ring, bridged to the cubane by four 4.221 phosphonates from both sides. Thus, there are no Co(II) ions directly linked to this cubane. In the corner of the $\{Co_2Ln_6O_8\}$ ring, both of the cobalt and lanthanide ions are bridged by a μ_3-hydroxide, which then bridges to a further cobalt(II) site. Thus, the $\{Co_6Gd_8\}$ core looks as if it grows two wings. However, for **12·Ni$_5$Gd$_8$**, one more Ni(II) bridged by two 5.222 phosphonates is directly attached to the $[Ni^{II}{}_3Gd^{III}(\mu_3\text{-}OH)_4]^{5+}$ cubane. This Ni(II) ion is further connected with a μ_3-OH group that bridges with two Gd(III) ions from the upper $\{NiGd_7O_8\}$ ring, closing the two wings of the core compared to the wing-opened $\{Co_6Gd_8\}$ core (Figure 5B). In addition to the support from phosphonates, there are two μ_3-hydroxides holding the two 3d metal ions of the cubane with four gadoliniums in the middle of the ring for both complexes. The average nearest M···Gd, Gd···Gd, and M···M separations in both the cubanes and the rings are (respectively) for **11·Co$_6$Gd$_8$**, about 3.50, 3.90, and 3.20 Å; for **12·Ni$_5$Gd$_8$**, 3.62, 3.87, and 3.12 Å.

Interestingly, in a similar synthetic procedure of **11·Co$_6$Gd$_8$**, we can isolate all the lanthanides heavier than Gd with identical $\{Co_6Ln_8\}$ (Ln = Gd, Dy, Tb, Er, Ho, Yb, and Y) core, whereas the isostructural compounds of **12·Ni$_5$Gd$_8$** only run over Sm to Tb. The lanthanides heavier than Dy result in a new but related structure, $[Ni_6Ln_8(\mu_3\text{-}OH)_8(\mu\text{-}OH_2)(O_3P\text{-}{}^tBu)_6(O_2C\text{-}{}^tBu)_{16}]$ (**12·Ni$_6$Ln$_8$**, Ln = Dy, Ho and Y) (Table S4). As shown in Figure 6, there is one additional Ni(II) center attached to the $\{NiLn_7O_8\}$ ring (Figure 6D) compared to **12·Ni$_5$Ln$_8$** (Ln = Sm to Tb). There is no obvious cause but rather a gradual change in the lanthanide ion radii for this alternation. The formation of this structure might be regarded as an intermediate phase between **12·Ni$_5$Ln$_8$** (Ln = Sm to Tb) and the **11·Co$_6$Ln$_8$** family. The core difference between **12·Ni$_6$Ln$_8$** (Ln = Dy, Ho, and Y) and **11·Co$_6$Ln$_8$** families lies only on the wing 3d metal ions, in which one side of the wing Ni(II) ion is closed and attached to the $\{Ni_3Ln\}$ cubane (Figure 6C) for the former family, but this linkage is broken in the latter. Except for this variation, the other parts, including the metal–metal distances and coordination geometries of the cores, are nearly identical for these two families.

2.1.4 | Cores with symmetry higher than C_3 (**13–15**)

Remarkably, when the numbers of 3d and 4f metals are equal, the shaped cores will have higher symmetry than C_3. As shown in Figure 7, these higher symmetric cores are aesthetically pleasing and can be described with mimic nick names. For example, the **13·Ni$_6$Gd$_6$** core has S_3 symmetry, which means that all the atoms after rotating 120°, followed by an inverse reflection to determine their equivalents. The shape of this $\{Ni_6Gd_6\}$ core is similar to a rugby (or American football), and if the phosphorus atoms are counted in this 18-member cage, $\{Ni_6Gd_6P_6\}$ also fits the definition of the well-known Wells–Dawson polyoxometallate.[23]

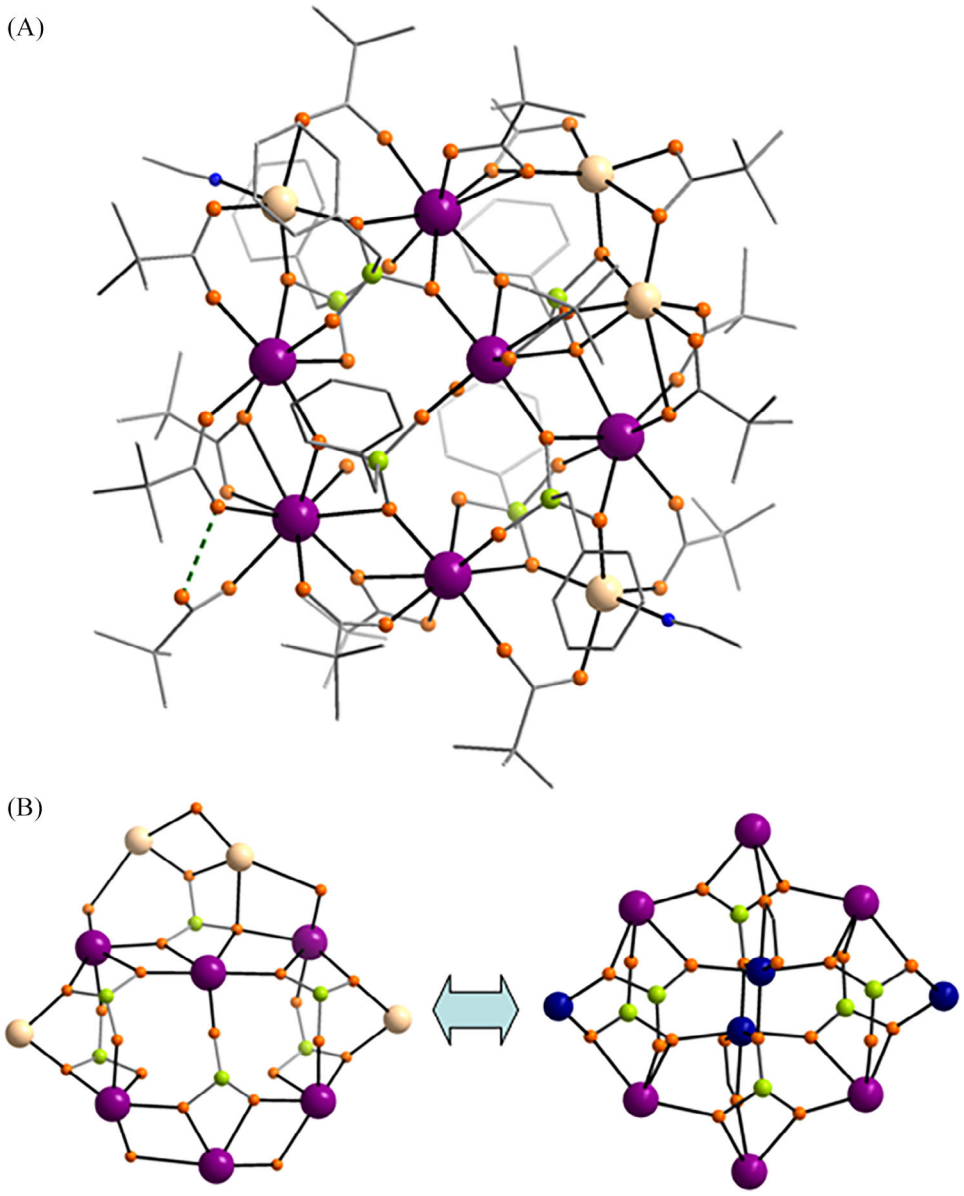

FIGURE 4 The molecular structure of **10**·Mn_4Gd_6 (A) and a comparison of the cores of **10**·Mn_4Gd_6 and **9**·Co_4Gd_6 (B).

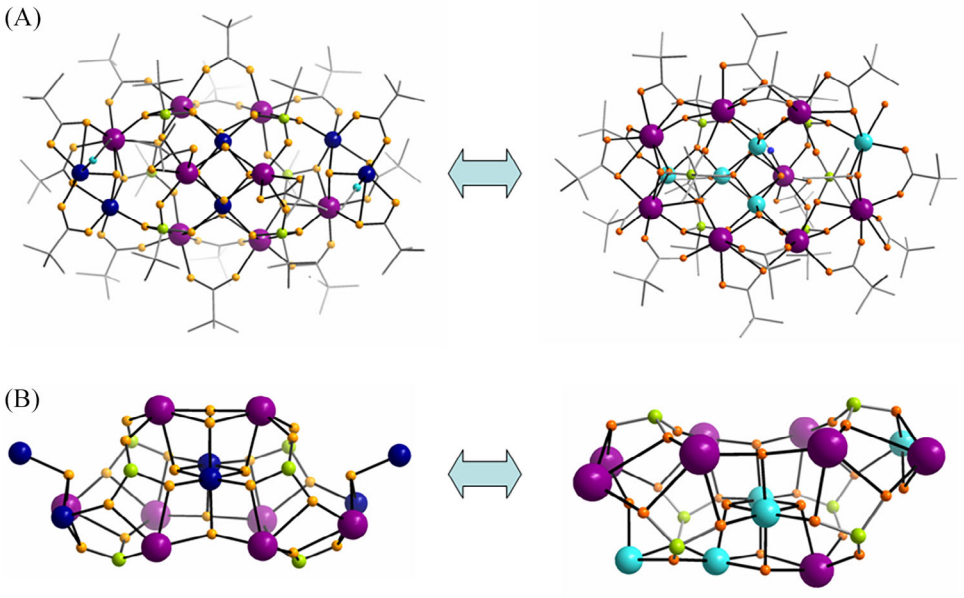

FIGURE 5 Comparisons of the molecular structures (A) and the cores (B) of **11**·Co_6Gd_8 and **12**·Ni_5Gd_8.

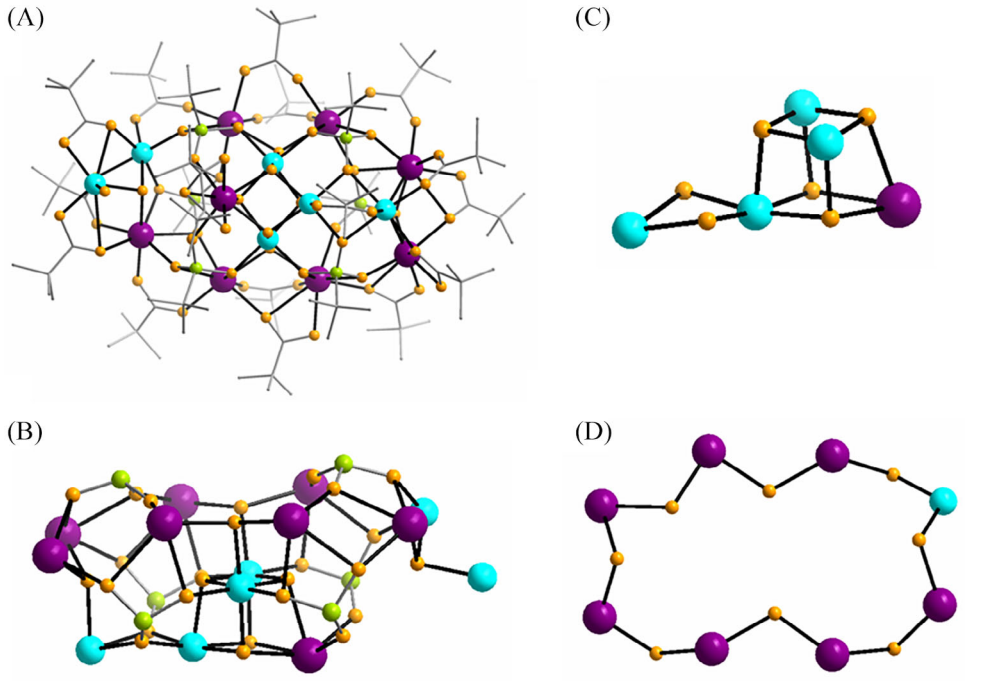

FIGURE 6 Structures of the molecule (A), the core (B), the central $\{Ni_4Ln\}$ unit (C) and the $\{NiLn_7O_8\}$ ring of the family **12·Ni$_5$Ln$_8$** (Ln = Dy, Ho, and Y) (D).

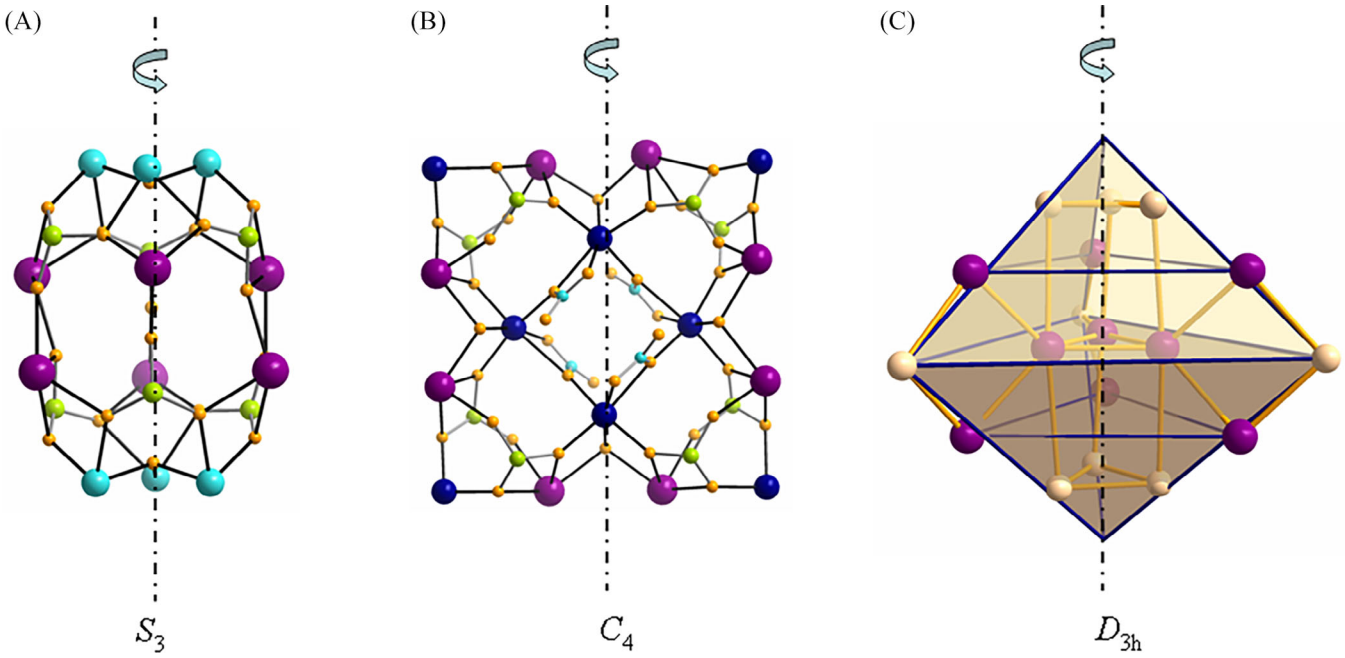

FIGURE 7 Cores with symmetry higher than C_3: **13·Ni$_6$Gd$_6$** (A), **14·Co$_8$Gd$_8$** (B), and **15·Mn$_9$Gd$_9$** (C).

The $\{Co_8Gd_8\}$ cage has a typical square-in-square structure, with an outer $\{Co_4Gd_8\}$ square that contains an inner $\{Co_4\}$ square. As such, the molecular square **14·Co$_8$Gd$_8$** has a four-fold rotational symmetry. However, due to the bending of the core, neither C_2 axis passes through the diagonals nor horizontal mirror lying in the plane. The highest symmetry in all these complexes occurs in the **15·Mn$_9$Gd$_9$** core, which has a threefold rotational axis going through the center of cluster, a middle horizontal mirror perpendicular to the C_3 axis, and three twofold axes with 120° next to each other in the horizontal mirror plane. Thus, the $\{Mn_9Gd_9\}$ core holds the D_{3h} symmetry, shaping a molecular diamond.

3 | MAGNETIC PROPERTIES

In addition to the complex **2·Ni$_2$Gd$_2$**, due to its low yield, magnetic properties of family **1–15** have been studied on polycrystalline samples. The obtained relevant information is summarized in Table 2, from which we can see that the room temperature effective magnetic moment (translated as the χT product because $\mu_{eff} = 2.83(\chi T)^{1/2}$) rises as both the 3d transition and Gd metal centers increase. However, the 2 K χT values diversify significantly due to the different magnetic exchange coupling interactions between these metal centers. In addition to the remarkable enhancement of the complex

TABLE 2 Magnetic data for the 3d-Gd mixed-metal complexes (**1–15**).

Compound	Obs. χT at 300 K ($cm^3\ mol^{-1}\ K$)	Obs. χT at 2 K ($cm^3\ mol^{-1}\ K$)	Obs. M at 2 K and at $7T$ (μ_B)	$-\Delta S_m$ at 3 K and at $7T$ ($J\ kg^{-1}\ K^{-1}$)	Gd% in molecular weight
1·Gd_2	15.8	14.9	13.91	21.6	20.5
2·Ni_2Gd_2	–	–	–	–	–
3·Fe_6Gd_2	27.0	14.6	12.8	4.4	11.5
4·$Fe_{17}Gd_2$	41.7	22.1	19.2	8.99	7.96
5·Co_4Gd_2	26.2	21.9	20.1	20.0	15.8
6·Co_8Gd_2	42.4	11.4	25.1	11.8	9.8
7·Co_8Gd_4	54.6	39.2	36.1	21.1	17.3
8·Mn_8Gd_4	66.9	32.2	50.5	22.7	17.8
9·Co_4Gd_6	61.6	46.5	79.3	23.6	25.5
10·Mn_4Gd_6	64.9	43.0	60.8	33.7	24.2
11·Co_6Gd_8	81.9	64.1	59.0	28.6	28.9
12·Ni_5Gd_8	69.8	86.7	64.8	30.6	30.7
13·Ni_6Gd_6	55.3	46.1	55.3	26.5	22.2
14·Co_8Gd_8	82.7	39.2	36.1	21.4	26.4
15·Mn_9Gd_9	104.2	64.3	80.9	28.0	27.9

12·Ni_5Gd_8, the overall 2 K χT products are lower than the room temperature ones, which are usually ascribed to ferro- or antiferromagnetic interactions, respectively. The following four representative examples were selected for detailed graphical analyses.

As shown in Figure 8A, the gradual descending χT versus T plot of **1·Gd_2** represents a very weakly coupled system.[24] There is only 1.0 $cm^3\ mol^{-1}$ K difference compared with the room temperature and 2 K values. Similarly, although rare in these series of complexes, can be found in complex **5·Co_4Gd_2**. The progressive decrease in the χT versus T plot of **4·$Fe_{17}Gd_2$** (Figure 8B) represents a much stronger but antiferromagnetically coupled system. The shape of χT versus T plot is usually very steep for such systems, leading to a large gap between the room temperature and low-temperature values. The tick formed at very low temperatures (below 5 K) is normally due to the presence of trace paramagnetic impurities.[25] The strong antiferromagnetic coupling is usually mediated by the single-atom oxo bridge. As such, this phenomenon is common in iron-containing systems (i.e., **4·$Fe_{17}Gd_2$** and **3·Fe_6Gd_2**, see also Figure S1), but less likely in other bridging systems such as hydroxy, carboxylato, and phosphonates. The moderate antiferromagnetic coupling system of **8·Mn_8Gd_4** represents the most common case among this series of complexes such as **6·Co_8Gd_2**, **7·Co_8Gd_4**, **11·Co_6Gd_8**, **14·Co_8Gd_8**, and **15·Mn_9Gd_9**. The χT versus T plot (Figure 8C) for such system usually decreases gradually within a higher temperature range and dramatically below certain point (i.e., 50 K). There is no upturn point in the χT versus T plot observed for such systems; nevertheless, with non-vanished values at 2 K, indicating a non-diamagnetic ground state. The rarest but most highly appreciated state of the χT versus T plot is the upward going one. As shown in Figure 8D, the χT versus T plot of **12·Ni_5Gd_8** exhibits such behavior, gradually increasing from 300 to 50 K, followed by a sharp increase. This is a very positive indication of ferromagnetic interaction or uncompensated magnetic moments from competing magnetic interactions, as observed in the complexes **9·Co_4Gd_6** and **13·Ni_6Gd_6**.[12] The latter shows a decrease in the χT versus T plot after reaching the maximum at 14 K.

The magnetic exchange coupling effect is also reflected in the isothermal magnetization (M) measurements (inserts of Figure 8). For stronger antiferromagnetic interaction systems (i.e., the complexes **3·Fe_6Gd_2** and **4·$Fe_{17}Gd_2$**), M shows a slower increase with increasing field (B) but does not saturate at $7T$. With less antiferromagnetic coupling, the increase in the M will be faster (i.e., the complex **8·Mn_8Gd_4**). The weakly coupled system features a paramagnetic behavior that could be well modeled by the Brillouin function (i.e., the complex **1·Gd_2**). For the ferromagnetically coupled system, the slopes of the M versus H plots are supposed to be even steeper at lower field (i.e., complex **12·Ni_5Gd_8**). In other words, they are more easily magnetized, which is critical in magnetic cooling applications.

This behavior is reflected well in the MCE, specifically in the entropy changes (ΔS_m) calculated from the Maxwell equation $\Delta S_m(T)_{\Delta B} = \int[\partial M(T,B)/\partial T]_B dB$.[2] As shown in Figure 9, the resulting $-\Delta S_m$ versus T plots of both weakly coupled and ferromagnetically coupled systems **1·Gd_2** and **12·Ni_5Gd_8** increase gradually from 10 to 3 K, reaching a maximum of 21.6 and 30.6 $J\ kg^{-1}\ K^{-1}$ at $7T$, respectively. There is still no sign of a downturn, which means that the maximum of these two complexes should occur at a lower temperature for the investigated applied field changes. For the antiferromagnetically coupled systems **4·$Fe_{17}Gd_2$** and **8·Mn_8Gd_4**, the $-\Delta S_m$ versus T plots gradually increase, reaching respective maximum of 9.0 and 23 $J\ kg^{-1}\ K^{-1}$ at 4 K already. These behaviors are typical in antiferromagnetically coupled systems.

Previously, we studied the magnetothermal properties of a series of {Co_xGd_y} complexes, which presumably revealed the reliance of MCE on the Gd(III) percentage.[8o] In order to check whether this presumption is applicable for other 3d transition metals, we plotted $-\Delta S_m$ versus Gd%, as shown in Figure 10, from which we can see that this conclusion is not always correct, although the linear tendency with $-\Delta S_m = k \times Gd\% + b$ (where $k = 0.98(1)$ $J\ kg^{-1}\ K^{-1}$

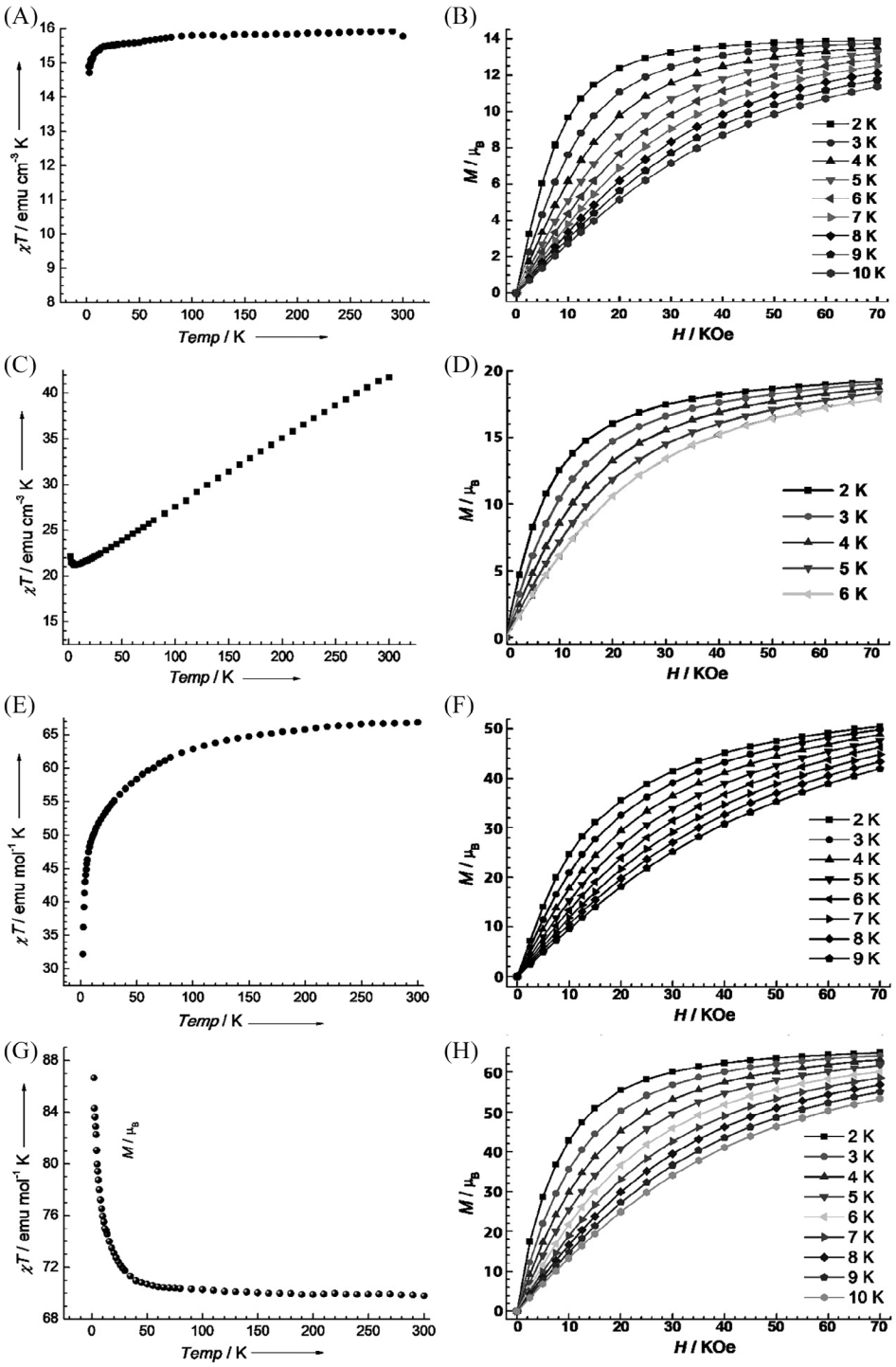

FIGURE 8 The χT versus T plot under 0.1T dc field and field-dependent magnetization plots at indicated temperatures of **1·Gd$_2$** (A and B), **4·Fe$_{17}$Gd$_2$** (C and D), **8·Mn$_8$Gd$_4$** (E and F), and **12·Ni$_5$Gd$_8$** (G and H), the lines are visual guides.

and b = 1.43(2) J kg^{-1} K^{-1}) is shown (red dashed line). For example, the compound **10·Mn$_4$Gd$_6$** with highest $-\Delta S_m$ does not have the most Gd(III) percentage, but the bottom complex **3·Fe$_6$Gd$_2$** has an even greater Gd% than complexes **4·Fe$_{17}$Gd$_2$** and **6·Co$_8$Gd$_2$**. Indeed, these are very complicated systems as each molecule is different from each other. Any simple relationship might lead to a wrong conclusion. For example, calculated as the maximum attainable $-\Delta S_m = R \ln(2s + 1)$, free magnetic ions such as Gd^{3+} (s = 7/2, fw = 157.25), Mn^{2+} (s = 5/2, fw = 54.94), Fe^{3+} (s = 5/2, fw = 55.85), Co^{2+} (s = 3/2, fw = 58.93), and Ni^{2+} (s = 1, fw = 58.69) will have $-\Delta S_m$ (J kg^{-1} K^{-1}) values of 109.9, 271.1, 266.7, 195.6, and 155.6, respectively. In fact, all these free 3d transition metals are supposed to have higher mass entropy changes as calculated. A reverse prediction was made compared to our previous studies of the {Co_xGd_y} complexes.[80] The magnetic interactions between the 3d metal centers and/or 3d-Gd metal centers are thus very important to the final net MCE of each complex.

Nevertheless, it is interesting to see that the linear dashed line is just going through the weakly coupled complex **1·Gd$_2$**, which can potentially serve as a reference for comparisons. Taking the {Gd_2}-containing family, for example, the introduction of other 3d transition metals, such as Co(II) and Fe(III), obviously negatively affects the enhancement of the MCE, as we can see that the $-\Delta S_m$ values of **5·Co$_4$Gd$_2$**,

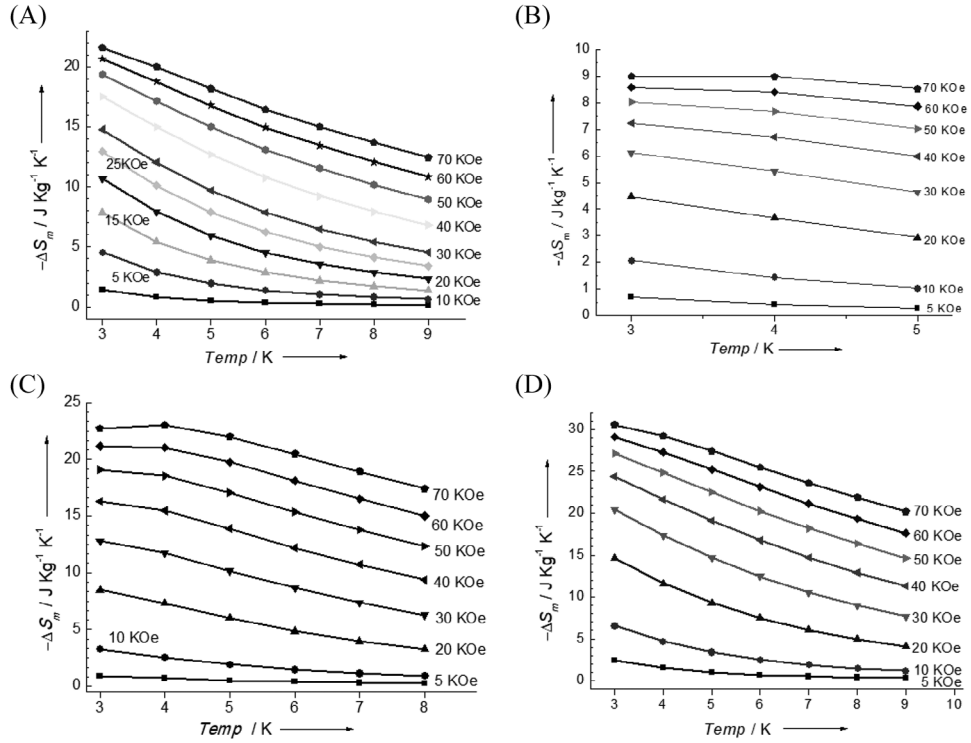

FIGURE 9 Experimental ΔS_m for **1·Gd$_2$** (A), **4·Fe$_{17}$Gd$_2$** (B), **8·Mn$_8$Gd$_4$** (C), and **12·Ni$_5$Gd$_8$** (D) at various fields and temperatures. Lines are guides to the eye.

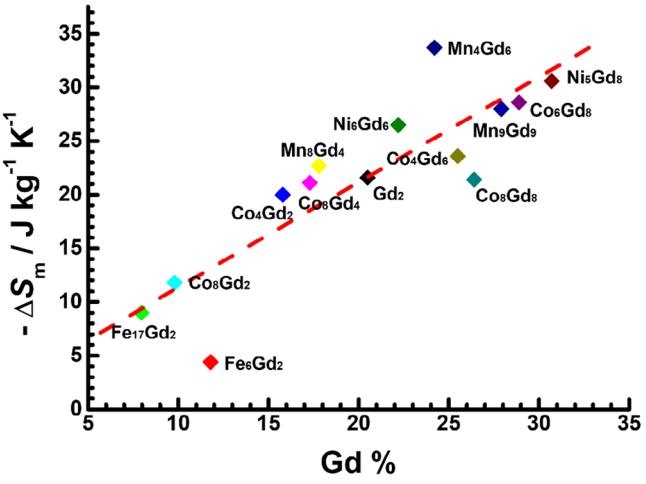

FIGURE 10 Experimental $-\Delta S_m$ versus Gd% for various 3d-Gd compounds. Dashed line: linear fit of the data.

6·Co$_8$Gd$_2$, **4·Fe$_{17}$Gd$_2$**, and **3·Fe$_6$Gd$_2$** are all below the entropy change of **1·Gd$_2$**, which may due to the dominant antiferromagnetic interactions between the metal centers. Another fact is the formation of spin-frustrated geometries such as {Fe$_3$(μ_3-O)} triangles and {Fe$_4$(μ_4-O)} tetrehedra. The former geometry, however, cannot explain the bottomed $-\Delta S_m$ value of complex **3·Fe$_6$Gd$_2$**. We therefore speculate that the tetrahedral {Fe$_4$(μ_4-O)} is vital for the enhancement of MCE, as the similar effect occurs in the **13·Ni$_6$Gd$_6$** complex due to the frustrated {Ni$_3$(μ_3-OH)} triangles.[12] However, further evidence is required.

If the direct proportional relation of $-\Delta S_m$ versus Gd% is effective for these complexes, the conclusion might simply be that antiferromagnetic couplings dominate between the 3d metal centers, which is actually in accordance with our previous magnetic fitting of the **13·Ni$_6$Y$_6$** complex,[12] in which the nickel centers are antiferromagnetically coupled despite the observation of an increasing χT versus T plot. A similar situation is probably applicable to the complex **12·Ni$_5$Gd$_8$**, implying that the magnetic interaction may be far more complicated than the presumably ferromagnetic coupling.

In other words, although Figure 10 indicates a nearly linear correlation between $-\Delta S_m$ and Gd%, this should be valid only for this special family. As mentioned above, the magnitude of $-\Delta S_m$ is governed by not only the magnetic interaction but also the density of magnetic moments. The former factor obviously outweighs the latter because the predicted entropy change in each 3d transition metal ion will have higher values than the single Gd(III) ion. In this consideration, the proper combination of Gd(III) and other 3d ions can generate a greater net entropy change than the pure Gd(III) ion does, which virtually offers a variety of future endeavoring directions for better MCE materials. However, due to the extremely difficult rational design of ferromagnetic interactions, the separation of the magnetic couplings between the 3d metal ions is more practical for enhancing MCE, and this is probably the reason that complex **10·Mn$_4$Gd$_6$** has the largest MCE in all the series.

4 | HEAT CAPACITY

In order to further investigate the largest observed magnetothermal effect of **12·Ni$_5$Gd$_8$**, we have performed heat capacity C experiments, which represent the best experimental tool for the assessment of the MCE.[7] Figure 11 shows the dependence of the heat capacity on temperature

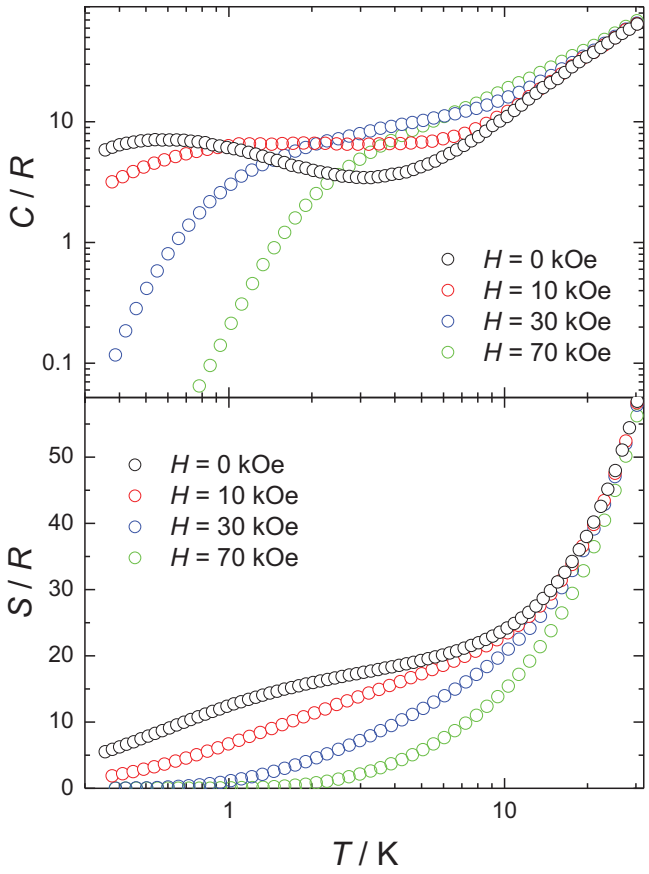

FIGURE 11 Top: molar specific heat versus temperature for **12·Ni$_5$Gd$_8$** at several applied fields, as labeled. Bottom: total entropy for **12·Ni$_5$Gd$_8$** normalized to the gas constant *R*.

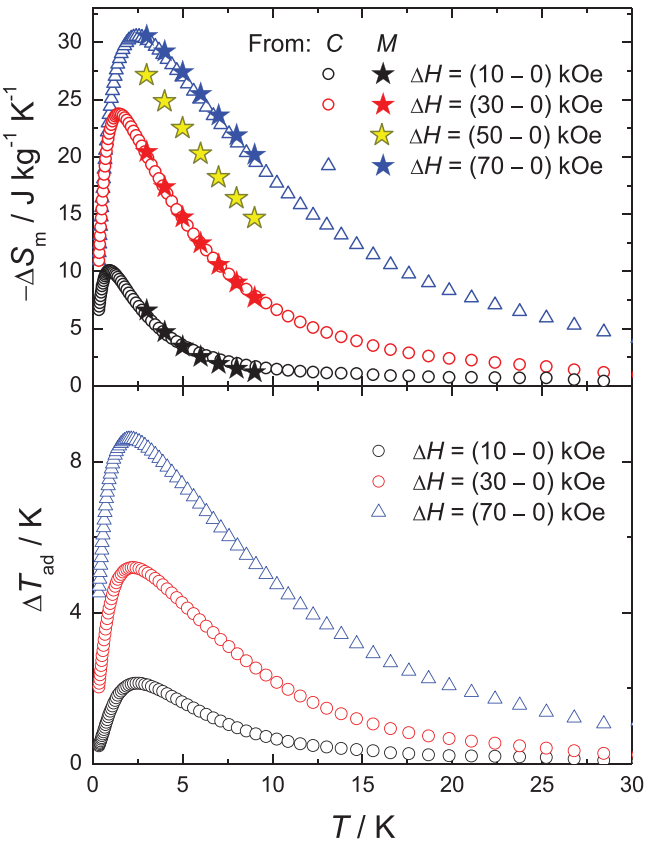

FIGURE 12 Top: temperature dependence of the magnetic entropy change for **12·Ni$_5$Gd$_8$** as obtained from heat capacity. The ΔS_m deduced from the magnetization data is also plotted for comparison. Bottom: adiabatic temperature change of **12·Ni$_5$Gd$_8$** corresponding to the indicated magnetic field changes, as obtained from heat capacity data.

for **12·Ni$_5$Gd$_8$**, collected at 0.35 K < *T* < 30 K and applied fields B_0 = 0, 1, 3, and 7*T*. Especially at the lowest temperature, it can be seen that the experimental curves are strongly dependent on the applied field, while in the high-temperature range, a large field-independent contribution appears that can be attributed to the lattice phonon modes of the crystal.

The entropy *S* of **12·Ni$_5$Gd$_8$** at the corresponding fields and temperatures (Figure 11) is then obtained from the heat capacity data by making use of the expression $S = \int C/T \mathrm{d}T$. From this result, it becomes straightforward to obtain the figures of merit of the MCE (Figure 12), that is, the adiabatic temperature change ΔT_{ad} and the magnetic entropy change ΔS_m for the selected field changes that we compare with the ΔS_m deduced from the magnetization data of **12·Ni$_5$Gd$_8$**.

The so-obtained ΔS_m curves of **12·Ni$_5$Gd$_8$** are consistent with the estimates depicted in Figure 9, proving the validity of employing both magnetization and heat capacity data in the analysis. In addition, the latest results extend our previous estimates, both for temperature and applied field change. Remarkably, the adiabatic temperature changes and the magnetic entropy change reach large values below liquid–helium temperature (Figure 12), for example, ΔT_{ad} = 8.6 K at 2.1 K and $-\Delta S_m$ = 30.9 J kg^{-1} K^{-1} at 2.5 K, respectively, for the investigated field change, ΔB_0 from 7 to 0*T*. The field-dependent maxima in $-\Delta S_m$ gradually approach the full available entropy of **12·Ni$_5$Gd$_8$**, which corresponds to the sum of the entropy of five uncorrelated Ni(II) and eight uncorrelated Gd(III) spins, that is, $5 \times R \ln(2s_{Ni} + 1) + 8 \times R \ln(2s_{Gd} + 1) = 22.1R = 41.8$ J kg^{-1} K^{-1}. The MCE reaches a high $-\Delta S_m$ = 10.7 J kg^{-1} K^{-1} at 1 K for low-field change (ΔB_0 from 1 to 0*T*), which exceeds most reported 3d-Gd-based polymetallic clusters and Gd-based clusters (Table S5).

5 | CONCLUSION

To summarize, by using 3d transition metals and gadolinium pivalates as major starting materials to react with different phosphonates, we obtained a range of 3d-Gd mixed-metal complexes with 15 types of cores: {Gd_2}, {Ni_2Gd_2}, {Co_4Gd_2}, {Co_8Gd_2}, {Fe_6Gd_2}, {$Fe_{17}Gd_2$}, {Co_8Gd_4}, {Mn_8Gd_4}, {Co_4Gd_6}, {Mn_4Gd_6}, {Co_6Gd_8}, {Ni_5Gd_8}, {Ni_6Gd_6}, {Co_8Gd_8}, and {Mn_9Gd_9}. From the structural point of view, six of the total 15 families have two Gd(III) ions, and the others have more Gd(III) metal centers. The last three families with equal 3d and Gd metal numbers show aesthetically pleasing cores with high symmetry. In most of these families, the lanthanide can be replaced by other heavier ones without alternating the structure except for the {Co_4Gd_6} and {Ni_5Gd_8} complexes, whose cores change after dysprosium, leading to the formation of new {Co_4Ln_6} and {Ni_6Ln_8} families. Note that the diversity of these discrete structures has not been realized in the coordination chemistry of phosphonates[26–29] until the solvothermal synthetic technique was first introduced into this mixed-metal system by us.[30]

Systematic investigations of these 3d-Gd heterometallic complexes with the use of different phosphonate offer a unique opportunity to study the effect of magnetic interactions on MCE. The different topologies and molecular weights of phosphonate ligands can not only influence the final architecture of 3d–4f clusters so as to affect the magnetic coupling among the metal centers, but also have some effect on the magnetic density of the products. Our previous study of series of $\{Co_xGd_y\}$ complexes revealed the direct proportional weight percentage of Gd(III) ions on MCE.[8o] With the whole series of 3d-Gd complexes, the conclusion, albeit is similar, is contrary to the prediction of the larger MCE for 3d transition metal ions. This reveals that antiferromagnetic interactions are dominated among the magnetic exchange couplings of the 3d metal and/or 3d-Gd metal centers. Besides, geometrically frustration in tetrahedral $\{Fe_4(\mu_4\text{-O})\}$ and triangular $\{Ni_3(\mu_3\text{-OH})\}$ motifs is promising for enhancing MCE; otherwise, weakly coupled systems are preferred if the metal centers are antiferromagnetically coupled. Although ferromagnetic interaction is supposed to have a positive response for better MCE, it is rare in these phosphonate-bridged mixed-metal complexes. The seemingly ferromagnetically coupled complexes **12·Ni$_5$Gd$_8$** and **13·Ni$_6$Gd$_6$** are dropped behind the fairly coupled **10·Mn$_4$Gd$_6$** value, suggesting that we can determine whether the metal centers in this complex are genuinely ferromagnetically coupled. In summary, this investigation reveals that the MCE is simultaneously correlated with both the Gd(III) percentage and the magnetic couplings among the metal centers. For a better MCE material, both factors should be balanced.

ACKNOWLEDGMENTS

This work was supported by the National Natural Science Foundation of China (nos. 21971203 and 22375157), the State Key Laboratory of Electrical Insulation and Power Equipment (nos. EIPE23402 and EIPE23405), the Special Support Plan of Shaanxi Province for Young Top-notch Talent and the Fundamental Research Funds for Central Universities (grant no. xtr052023002), the Medical-Engineering Cross Project of the First Affiliated Hospital of XJTU (QYJC02), the Spanish MICINN (no. PID2021-124734OB-C21), and the "Scientists + Engineers" Team Building Project of Qin Chuang Yuan (2022KXJ-088). We thank Simon J. Teat (Lawrence Berkeley National Lab) for helping with the synchrotron X-ray crystallography and Prof. Richard E.P. Winpenny (University of Manchester) for helpful discussion and assistance from the Instrument Analysis Center of Xi'an Jiaotong University.

CONFLICT OF INTEREST STATEMENT

The authors declare they have no conflicts of interest.

ORCID

Marco Evangelisti https://orcid.org/0000-0002-8028-9064
Yan-Zhen Zheng https://orcid.org/0000-0003-4056-097X

REFERENCES

1. a) P. Weiss, A. Piccard, *J. Phys. Theor. Appl.* **1917**, *7*, 103; b) A. Smith, *Eur. Phys. J. H* **2013**, *38*, 507.
2. a) C. Zimm, A. Jastrab, A. Sternberg, V. Pecharsky, K. A. Gschneidner Jr., M. Osborne, I. Anderson, *Adv. Cryog. Eng.* **1998**, *43*, 1759; b) V. Pecharsky, K. A. Gschneidner Jr., *J. Magn. Magn. Mater.* **1999**, *200*, 44; c) F. B. Yu, Q. Gao, B. Zhang, X. Z. Meng, Z. Chen, *Inter. J. Refrigeration* **2003**, *26*, 622; d) V. Pecharsky, K. A. Gschneidner Jr., *Inter. J. Refrigeration* **2006**, *29*, 1239; e) K. A. Gschneidner Jr., V. Pecharsky, *Inter. J. Refrigeration* **2008**, *31*, 945.
3. a) J. A. Barclay, W. A. Steyert, *Cryogenics* **1982**, *22*, 73; b) A. M. Tishin, Y. I. Spichkin, *The Magnetocaloric Effect and its Applications*, Institute of Physics Publishing, Bristols **2003**; (c) S. W. Van Sciver, *Helium Cryogenics*, 2nd ed., Springer, New York **2012**.
4. V. K. Pecharsky, K. A. Gschneidner Jr., *Phys. Rev. Lett.* **1997**, *78*, 4499.
5. B. Daudin, R. Lagnier, B. J. Salce, *Magn. Magn. Mater.* **1982**, *27*, 315.
6. R. D. McMichael, J. J. Ritter, R. D. Shull, *J. Appl. Phys.* **1993**, *73*, 6946.
7. a) R. Sessoli, D. Gatteschi, J. Villain, *Molecular Nanomagnets*, Oxford University Press, Oxford **2006**; b) G. Christou, D. Gatteschi, D. N. Hendrickson, R. Sessoli, *MRS Bull.* **2000**, *25*, 66; c) D. Gatteschi, R. Sessoli, *Angew. Chem. Int. Ed.* **2003**, *43*, 268; d) G. Aromí, E. K. Brechin, *Struct. Bonding* **2006**, *122*, 1.
8. a) M. Evangelisti, F. Luis, L. J. de Jongh, M. J. Affronte, *Mater. Chem.* **2006**, *16*, 2534; b) M. Manoli, R. D. L. Johnstone, S. Parsons, M. Murrie, M. Affronte, M. Evangelisti, E. K. Brechin, *Angew. Chem. Int. Ed.* **2007**, *46*, 4456; c) M. Manoli, A. Collins, S. Parsons, A. Candini, M. Evangelisti, E. K. Brechin, *J. Am. Chem. Soc.* **2008**, *130*, 11129; d) G. Karotsis, M. Evangelisti, S. J. Dalgarno, E. K. Brechin, *Angew. Chem. Int. Ed.* **2009**, *48*, 9928; e) M. Evangelisti, A. Candini, M. Affronte, E. Pasca, L. J. de Jongh, R. T. W. Scott, E. K. Brechin, *Phys. Rev. B* **2009**, *79*, 104414; f) M. Evangelisti, E. K. Brechin, *Dalton Trans.* **2010**, *39*, 4672; g) S. Nayak, M. Evangelisti, A. K. Powell, J. Reedijk, *Chem. Eur. J.* **2010**, *43*, 12865; h) G. Karotsis, S. Kennedy, S. J. Teat, C. M. Beavers, D. A. Fowler, J. J. Morales, M. Evangelisti, S. J. Dalgarno, E. K. Brechin, *J. Am. Chem. Soc.* **2010**, *132*, 12983; i) S. K. Langley, N. F. Chilton, B. Moubaraki, T. Hooper, E. K. Brechin, M. Evangelisti, K. S. Murray, *Chem. Sci.* **2011**, *2*, 1166; j) P. B. Jin, Q. C. Luo, X. J. Kong, Y. P. Ren, L. S. Long, R. B. Huang, L. S. Zheng, Z. Zheng, *Angew. Chem. Int. Ed.* **2011**, *50*, 10649; k) J. W. Sharples, Y. Z. Zheng, F. Tuna, E. J. L. McInnes, D. Collison, *Chem. Commun.* **2011**, *47*, 7650; l) Y. Z. Zheng, M. Evangelisti, R. E. P. Winpenny, *Chem. Sci.* **2011**, *2*, 99; m) M. Evangelisti, O. Roubeau, E. Palacios, A. Camón, T. N. Hooper, E. K. Brechin, J. J. Alonso, *Angew. Chem. Int. Ed.* **2011**, *50*, 6606; n) P. B. Jin, Q. C. Luo, X. J. Kong, Y. Z. Zheng, Y. P. Ren, L. S. Long, R. B. Huang, L. S. Zheng, Y. Z. Zheng, *J. Am. Chem. Soc.* **2012**, *134*, 3314; o) Y. Z. Zheng, M. Evangelisti, F. Tuna, R. E. P. Winpenny, *J. Am. Chem. Soc.* **2012**, *134*, 1057; p) Y. Z. Zheng, E. M. Pineda, M. Helliwell, R. E. P. Winpenny, *Chem. Eur. J.* **2012**, *18*, 4161; q) S. J. Liu, J. P. Zhao, J. Tao, J. M. Jia, S. D. Han, Y. Li, Y. C. Chen, X. H. Bu, *Inorg. Chem.* **2013**, *52*, 9163; r) K. Wang, Z. L. Chen, H. H. Zou, K. Hu, H. Y. Li, Z. Zhang, W. Y. Sun, F. P. Liang, *Chem. Commun.* **2016**, *52*, 8297.
9. a) L. Sedláková, J. Hanko, A. Orendáčová, M. Orendáč, C. L. Zhou, W. H. Zhu, B. W. Wang, Z. M. Wang, S. Gao, *J. Alloys Compd.* **2009**, *487*, 425; b) F. S. Guo, Y. C. Chen, J. L. Liu, J. D. Leng, Z. S. Meng, P. Vrábel, M. Orendáč, M. L. Tong, *Chem. Commun.* **2012**, *48*, 12219; c) P. F. Shi, Y. Z. Zheng, X. Q. Zhao, G. Xiong, B. Zhao, F. F. Wan, P. Cheng, *Chem. Eur. J.* **2012**, *18*, 15086; d) G. Lorusso, M. A. Palacios, G. S. Nichol, E. K. Brechin, O. Roubeau, M. Evangelisti, *Chem. Commun.* **2012**, *48*, 7592; e) R. Sibille, T. Mazet, B. Malaman, M. François, *Chem. Eur. J.* **2012**, *18*, 12970; f) F.-S. Guo, Y.-C. Chen, L.-L. Mao, W.-Q. Lin, J.-D. Leng, R. Tarasenko, M. Orendáč, J. Prokleška, V. Sechovský, M.-L. Tong, *Chem. Eur. J.* **2013**, *19*, 14876; g) J. W. Sharples, D. Collison, *Polyhedron* **2013**, *54*, 91; h) L.-X. Chang, G. Xiong, L. Wang, P. Cheng, B. Zhao, *Chem. Commun.* **2013**, *49*, 1055; i) J.-B. Peng, X.-J. Kong, Q.-C. Zhang, M. Orendáč, J. Prokleška, Y.-P. Ren, L.-S. Long, Z. Zheng, L.-S. Zheng, *J. Am. Chem. Soc.* **2014**, *136*, 17938; j) W.-P. Chen, P.-Q. Liao, Y. Yu, Z. Zheng, X.-M. Chen, Y.-Z. Zheng, *Angew. Chem. Int. Ed.* **2016**, *55*, 9375; k) X.-Y. Zheng, Y.-H. Jiang, G.-L. Zhuang, D.-P. Liu, H.-G. Liao, X.-J. Kong, L.-S. Long, L.-S. Zheng, *J. Am. Chem. Soc.* **2017**, *139*, 18178; l) W.-P. Chen, P.-Q. Liao, P.-B. Jin, L. Zhang, B.-K. Ling, S.-C. Wang, Y.-T. Chan, X.-M. Chen, Y.-Z. Zheng, *J. Am. Chem. Soc.* **2020**, *142*, 4663; m) Z. Lu, Z. Zhuo, W. Wang, Y.-G. Huang, M. Hong, *Inorg. Chem. Front.* **2023**, *10*, 979; n) M.-H. Du, D.-H. Wang, L.-W. Wu, L.-P. Jiang, J.-P. Li, L.-S. Long, L.-S. Zheng, X.-J. Kong, *Angew. Chem. Int. Ed.* **2022**, *61*, e2022005; o) N.-F. Li, Y.-M Han, J.-N. Li, Q. Chen, Y. Xu, *Dalton Trans.* **2022**, *51*, 2669; p) W.-P. Chen, J. Singleton, L. Qin, A. Camón, L. Engelhardt, F. Luis, R. E. P. Winpenny, Y.-Z. Zheng, *Nat. Commun.*

2018, *9*, 2107; q) N. Li, Q. Lin, Y. Han, Z. Du, Y. Xu, *Chin. Chem. Lett.* **2021**, *32*, 3808; r) E. M. Pineda, F. Tuna, R. G. Pritchard, A. C. Regan, R. E. P. Winpenny, E. J. McInnes, *Chem. Commun.* **2013**, *49*, 3522; s) Y. Zheng, Q.-C. Zhang, L.-S. Long, R.-B. Huang, A. Müller, J. Schnack, Z.-P. Zheng, *Chem. Commun.* **2013**, *49*, 36; t) T. G. Tziotzi, D. Gracia, S. J. Dalgarno, J. Schnack, M. Evangelisti, E. K. Brechin, C. J. Milios, *J. Am. Chem. Soc.* **2023**, *145*, 7743; u) Q. Xu, B. Liu, M. Ye, G. Zhuang, L. Long, L. Zheng, *J. Am. Chem. Soc.* **2022**, *144*, 13787; v) C. Delacotte, T. A. Pomelova, T. Stephant, T. Guizouarn, S. Cordier, N. G. Naumov, P. Lemoine, *Chem. Mater.* **2022**, *34*, 1829; w) E. C. Koskelo, C. Liu, P. Mukherjee, N. D. Kelly, S. E. Dutton, *Chem. Mater.* **2022**, *34*, 3440; x) Z. Yang, J.-Y. Ge, S. Ruan, H. Cui, Y.-J. Zeng, *J. Mater. Chem. C* **2021**, *9*, 6754.

10. a) Yu. I. Spichkin, A. K. Zvezdin, S. P. Gubin, A. S. Mischenko, A. M. Tishin, *J. Phys. D: Appl. Phys.* **2001**, *34*, 1162; (b) X. X. Zhang, H. L. Wei, Z. Q. Zhang, L. Zhang, *Phys. Rev. Lett.* **2001**, *87*, 157203; c) J. Schnack, R. Schmidt, J. Richter, *Phys. Rev. B* **2007**, *76*, 054413.
11. a) M. Evangelisti, A. Candini, A. Ghirri, M. Affronte, E. K. Brechin, E. J. L. McInnes, *Appl. Phys. Lett.* **2005**, *87*, 072504; b) R. Shaw, R. H. Laye, L. F. Jones, D. M. Low, C. Talbot-Eeckelaers, Q. Wei, C. J. Milios, S. Teat, M. Helliwell, J. Raftery, M. Evangelisti, M. Affronte, D. Collison, E. K. Brechin, E. J. L. McInnes, *Inorg. Chem.* **2007**, *46*, 4968.
12. Y. Z. Zheng, M. Evangelisti, R. E. P. Winpenny, *Angew. Chem. Int. Ed.* **2011**, *50*, 3692.
13. T. N. Hooper, J. Schnack, S. Piligkos, M. Evangelisti, E. K. Brechin, *Angew. Chem. Int. Ed.* **2012**, *51*, 4633.
14. a) A. J. Tasiopoulos, W. Wernsdorfer, B. Moulton, M. J. Zaworotko, G. Christou, *J. Am. Chem. Soc.* **2003**, *125*, 15274; b) A. Mishra, W. Wernsdorfer, K. A. Abboud, G. Christou, *J. Am. Chem. Soc.* **2004**, *126*, 15648; c) A. Mishra, W. Wernsdorfer, K. A. Abboud, G. Christou, T. C. Stamatatos, S. J. Teat, W. Wernsdorfer, G. Christou, *Angew. Chem. Int. Ed.* **2009**, *48*, 521; d) C. Papatriantafyllopoulou, W. Wernsdorfer, K. A. Abboud G. Christou, *Inorg. Chem.* **2011**, *50*, 421.
15. a) S. Osa, T. Kido, N. Matsumoto, N. Re, A. Pochaba, J. Mrozinski, *J. Am. Chem. Soc.* **2004**, *126*, 420; b) C. M. Zaleski, E. C. Depperman, J. W. Kampf, M. L. Kirk, V. L. Pecoraro, *Angew. Chem. Int. Ed.* **2004**, *43*, 3912; c) A. Mishra, W. Wernsdorfer, S. Parsons, G. Christou, E. K. Brechin, *Chem. Commun.* **2005**, 2086, https://doi.org/10.1039/B501508A; d) C. Aronica, G. Pilet, G. Chastanet, W. Wernsdorfer, J. F. Jacquot, D. Luneau, *Angew. Chem. Int. Ed.* **2006**, *45*, 4659; e) F. Mori, T. Nyui, T. Ishida, T. Nogami, K. Y. Choi, H. Nojiri, *J. Am. Chem. Soc.* **2006**, *128*, 1440; f) V. M. Mereacre, A. M. Ako, R. Clérac, W. Wernsdorfer, G. Filoti, J. Bartolome, C. E. Anson, A. K. Powell, *J. Am. Chem. Soc.* **2007**, *129*, 9248; g) F. Pointillart, K. Bernot, R. Sessoli, D. Gatteschi, *Chem. Eur. J.* **2007**, *13*, 1602; h) V. Mereacre, A. M. Ako, R. Clerac, W. Wernsdorfer, I. J. Hewitt, C. E. Anson, A. K. Powell, *Chem. Eur. J.* **2008**, *14*, 3577; i) M. N. Akhtar, Y. Z. Zheng, Y. Lan, V. Mereacre, C. E. Anson, A. K. Powell, *Inorg. Chem.* **2009**, *48*, 3502; j) S. Langley, B. Moubaraki, Murray, K. S. *Dalton Trans*. **2010**, *39*, 5066; k) V. Mereacre, Y. Lan, R. Clerac, A. M. Ako, I. J. Hewitt, W. Wernsdorfer, G. Buth, C. E. Anson, A. K. Powell, *Inorg. Chem.* **2010**, *49*, 5293; (l) C. M. Liu, D. Q. Zhang, D. B. Zhu, *Dalton Trans.* **2010**, *39*, 11325; m) T. Kajiwara, M. Nakano, K. Takahashi, S. Takaishi, M. Yamashita, *Chem. Eur. J.* **2011**, *17*, 196; n) J.-L. Liu, F. S. Guo, Z. S. Meng, Y. Z. Zheng, J. D. Leng, M. L. Tong, L. Ungur, L. F. Chibotaru, K. J. Heroux, D. N. Hendrickson, *Chem. Sci.* **2011**, *2*, 1268.
16. J. Schnack, R. Schmidt, J. Richter, *Phys. Rev. B* **2007**, *76*, 054413.
17. R. Sessoli, *Angew. Chem. Int. Ed.* **2012**, *51*, 43.
18. a) G. Aromi, A. S. Batsanov, P. Christian, M. Helliwell, A. Parkin, S. Parsons, A. A. Smith, G. A. Timco, R. E. P. Winpenny, *Chem. Eur. J.* **2003**, *9*, 5142; b) I. G. Fomina, M. A. Kiskin, A. G. Martynov, G. G. Aleksandrov, Z. V. Dobrokhotova, Y. G. Gorbunova, Y. G. Shvedenkov, A. Y. Tsivadze, V. M. Novotortsev, I. L. Eremenko, *Zh. Neorg. Khim.* **2004**, *49*, 1463.
19. Harris notation describes the binding mode as [X.Y_1Y_2…Y_n] where X is the overall number of metal bound by the whole ligand, and each value of Y refers to the number of metal atoms attached to the different donor atoms. See also R. A. Coxall, S. G. Harris, D. K. Henderson, S. Parsons, P. A. Tasker, R. E. P. Winpenny, *J. Chem. Soc., Dalton Trans.* **2000**, 2349.
20. a) J. Reuben, in *Handbook on Physics and Chemistry of Rare Earths* (Eds: K. A. Gschneidner Jr., L. Eyring), Vol. *4*, North-Holland, Amsterdam **1979**, p. 515; b) R. Wang, F. Gao, T. Jin, *Huaxue Tongbao* **1996**, *10*, 14, and references therein; c) R. Wang, H. Liu, D. M. Carducci, T. Jin, C. Zheng, Z. Zheng, *Inorg. Chem.* **2001**, *40*, 2743.
21. A. J. Belsky, T. B. Brill, *J. Phys. Chem. A* **1999**, *103*, 3006.
22. R. E. P. Winpenny, *J. Chem. Soc., Dalton Trans.* **2002**, 1. https://doi.org/10.1039/B107118C.
23. a) A. Müller, E. Krickemeyer, H. Bögge, M. Schmidtmann, F. Peters, *Angew. Chem. Int. Ed.* **1998**, *37*, 3359; b) A. Müller, S. Polarz, S. K. Das, E. Krickemeyer, H. Bögge, M. Schmidtmannm, B. Hauptfleisch, *Angew. Chem. Int. Ed.* **1999**, *38*, 3241; c) A. Müller, S. Sarkar, S. Q. N. Shah, H. Bögge, M. Schmidtmann, S. Sarkar, P. Kögerler, B. Hauptfleisch, A. X. Trautwein, V. Schünemann, *Angew. Chem. Int. Ed.* **1999**, *38*, 3238; d) A. Müller, S. Q. N. Shah, H. Bögge, M. Schmidtmann, P. Kögerler, B. Hauptfleisch, S. Leiding, K. Wittler, *Angew. Chem. Int. Ed.* **2000**, *39*, 1614; e) A. Müller, S. K. Das, M. Talismanova, H. Bögge, P. Kögerler, M. Schmidtmann, S. Talismanov, M. Luban, E. Krickemeyer, *Angew. Chem. Int. Ed.* **2002**, *41*, 579; f) A. M. Todea, A. Merca, H. Bögge, J. van Slageren, M. Dressel, L. Engelhardt, M. Luban, T. Glaser, M. Henry, A. Müller, *Angew. Chem. Int. Ed.* **2007**, *46*, 6106.
24. a) C. Benelli, D. Gatteschi, *Chem. Rev.* **2002**, *102*, 2369; b) L. Sorace, C. Benelli, D. Gatteschi, *Chem. Soc. Rev.* **2011**, *40*, 3092.
25. a) O. Kahn, *Molecular Magnetism*, VCH, New York **1993**; b) R. L. Carlin, *Magnetochemistry*, Springer, Berlin **1986**.
26. A. Clearfield, *Curr. Opin. Solid State Mater. Sci.* **1996**, *1*, 268 and references therein.
27. a) M. I. Khan, J. Zubieta, *Prog. Inorg. Chem.* **1995**, *43*, 1; b) V. Chandrasekhar, S. Kingsley, *Angew. Chem. Int. Ed.* **2000**, *39*, 2320; c) E. I. Tolis, M. Helliwell, S. Langley, J. Raftery, R. E. P. Winpenny, *Angew. Chem. Int. Ed.* **2003**, *42*, 3804; d) S. Maheswaran, G. Chastanet, S. J. Teat, T. Mallah, R. Sessoli, W. Wernsdorfer, R. E. P. Winpenny, *Angew. Chem. Int. Ed.* **2005**, *44*, 5044; e) S. J. Langley, M. Helliwell, R. Sessoli, P. Rosa, W. Wernsdorfer, R. E. P. Winpenny, *Chem. Commun.* **2005**, 5029. https://doi.org/10.1039/B510106A; f) S. Konar, N. Bhuvanesh, A. Clearfield, *J. Am. Chem. Soc.* **2006**, *128*, 9604; g) M. Shanmugam, G. Chastanet, T. Mallah, R. Sessoli, S. J. Teat, G. A. Timco, R. E. P. Winpenny, *Chem. Eur. J.* **2006**, *12*, 8777; h) S. Khanra, M. Kloth, H. Mansaray, C. A. Muryn, F. Tuna, E. C. Sanũdo, M. Helliwell, E. J. L. McInnes, R. E. P. Winpenny, *Angew. Chem. Int. Ed.* **2007**, *46*, 5568; i) Y.-S. Ma, Y. Song, Y.-Z. Li, L.M. Zheng, *Inorg. Chem.* **2007**, *46*, 5459; j) S. Langley, M. Helliwell, R. Sessoli, S. J. Teat, R. E. P. Winpenny, *Inorg. Chem.* **2008**, *47*, 497; k) V. Chandrasekhar, L. Nagarajan, R. Clérac, S. Ghosh, S. Verma, *Inorg. Chem.* **2008**, *47*, 1067; l) S. Konar, A. Clearfield, *Inorg. Chem.* **2008**, *47*, 3489; m) S. Konar, A. Clearfield, *Inorg. Chem.* **2008**, *47*, 5573; n) R. Murugavel, N. Gogoi, K. G. Suresh, S. Lavek, H. C. Verma, *Chem. Asian J.* **2009**, *4*, 923.
28. M. Wang, D. Q. Yuan, C. B. Ma, M. J. Yuan, M.-Q. Hu, N. Li, H. Chen, C. N. Chen, Q. T. Liu, *Dalton Trans.* **2010**, *39*, 7276.
29. V. Baskar, K. Gopal, M. Helliwell, F. Tuna, W. Wernsdorfer, R. E. P. Winpenny, *Dalton Trans.* **2010**, *39*, 4747.
30. a) B. A. Breeze, M. Shanmugam, F. Tuna, R. E. P. Winpenny, *Chem. Commun.* **2007**, 5185. https://doi.org/10.1039/B711650K; b) Y. Z. Zheng, B. A. Breeze, G. A. Timco, R. E. P. Winpenny, *Dalton Trans.* **2010**, *39*, 6175; c) Y. Z. Zheng, R. E. P. Winpenny, *Sci. China Chem.* **2012**, *55*, 910.

SUPPORTING INFORMATION

Additional supporting information can be found online in the Supporting Information section at the end of this article.

How to cite this article: Y.-Q. Zhai, W.-P. Chen, M. Evangelisti, Z. Fu, Y.-Z. Zheng, *Aggregate* **2024**, e520. https://doi.org/10.1002/agt2.520